Relationships between radionuclides, metals, and sediment properties in sediment of a bay exposed to anthropogenic pressure and mixed sediment sources (Kaštela Bay, Adriatic Sea, Croatia)

Ivanka Lovrenčić Mikelić [a,*], Višnja Oreščanin [b], Neven Cukrov [c], Nenad Tomašić [d], Mirta Rubčić [e], Delko Barišić [f]

[a] *Laboratory for Low-Level Radioactivities, Division of Experimental Physics, Ruđer Bošković Institute, Bijenička cesta 54, 10 000 Zagreb, Croatia, ivanka.lovrencic@irb.hr, +385-1-4560943*

[b] *Advanced Energy Ltd., V. Prekrata 43, 10 000 Zagreb, Croatia, vorescan@gmail.com*

[c] *Laboratory for Physical Chemistry of Traces, Division for Marine and Environmental Research, Ruđer Bošković Institute, Bijenička cesta 54, 10 000 Zagreb, Croatia, ncukrov@irb.hr*

[d] *Department of Geology, Faculty of Science, Horvatovac 102a, 10 000 Zagreb, Croatia, ntomasic@geol.pmf.hr*

[e] *Department of Chemistry, Faculty of Science, Horvatovac 102a, 10 000 Zagreb, Croatia, mirta@chem.pmf.hr*

[f] *Laboratory for Radioecology, Division for Marine and Environmental Research, Ruđer Bošković Institute, Bijenička cesta 54, 10 000 Zagreb, Croatia, dbarisic@irb.hr*

Highlights

- Predominant influencing parameters vary with sediment depth

* Corresponding author

- Significant anthropogenic impact on Cu, Zn, Pb, and ^{137}Cs
- ^{137}Cs introduction path into environment not differentiated
- ^{226}Ra and ^{238}U possibly separated by natural processes
- Mineral composition reveals fly and bottom ash deposition in the sea

Abstract

Natural and anthropogenic radionuclides, metals, organic matter, sediment grain size, mineral composition, and sediment sources were studied in marine sediment of Kaštela Bay up to a depth of 0.5 m. Deposition of man-modified material into the sea was evidenced in sediment mineral composition. Presence of pyrite and hematite in this sediment may pose an environmental concern. Metals, radionuclides, and organic matter were grouped in three groups: (i) variables under no anthropogenic influence and preferentially associated with carbonates (Ca, Sr); (ii) variables under no or weak anthropogenic influence and preferentially associated with aluminosilicates (Al, K, Ti, V, Cr, Mn, Fe, Co, Ni, Ga, Rb, Y, ^{40}K, ^{232}Th); (iii) variables under notable anthropogenic influence and/or natural processes of separation (Cu, Zn, Pb, As, ^{226}Ra, ^{238}U, ^{137}Cs, organic matter). Predominant influencing parameters change with sediment depth for some variables. Anthropogenic influence was the most emphasised for Cu, Zn, and Pb, followed by ^{137}Cs.

Keywords: Coastal zone; Flysch; Karst; Marine sediment; PCA; Radioactivity

1. Introduction

Metals and radionuclides (MAR), including both natural and anthropogenic radionuclides, in different environmental compartments have long been in scientific community focus because of their various anthropogenic and/or natural sources and potential

adverse effects on environment and human health in cases of their excessive accumulation (Aközcan and Uğur Görgün, 2013; Álvarez-Iglesias and Rubio, 2009; Aziman et al., 2021; Bobos et al., 2021; Feng et al., 1998; Fouskas et al., 2018; Külahcı and Şen, 2008; Liu et al., 2021, 2019; Lovrenčić Mikelić and Barišić, 2022a, 2022b; Lovrenčić Mikelić et al., 2021, 2013; Sauvé et al., 2021; Shahrokhi et al., 2021; Suresh et al., 2011; Topcuoğlu et al., 2003; Wanjeri et al., 2021). They have been studied either separately (more frequently) or together and a variety of environments (e.g. shallow or deep sea, coasts, lakes, rivers, watersheds, estuaries), sample types (e.g. marine sediment, coastal sand, lake sediment, river sediment, biota, water), and geological backgrounds (e.g. granites, metamorphic rocks, carbonates) has been encompassed. However, most of the previous researches were oriented to MAR's distribution, contamination/pollution, and/or risk assessment. They were also mostly limited on a few selected MAR. Relationships between metals only, radionuclides only, and between MAR were usually limited to Pearson correlation coefficients, while other statistical analyses were more rarely used (Liu et al, 2021; Lovrenčić Mikelić et al., 2021, 2013; Shahrokhi et al., 2021). Multivariate statistical analyses such as principal component analysis (PCA) were mostly used to differentiate natural and anthropogenic sources of MAR, rather than studying their relationships (Liu et al., 2021).

MAR in coastal areas were of special scientific interest since coastal areas are strongly exposed and are sensitive to anthropogenic activities, while coastal marine sediments may act as a sink or secondary source of MAR. Although numerous marine coastal areas with various geological backgrounds and differing anthropogenic influences were studied previously, no evidence was found that MAR relationships related to carbonate-flysch terrestrial rock association as geological background were studied, especially using statistical clustering techniques. This coastal terrestrial rock association serving as a provenance for marine sediments will influence MAR relationships in marine sediments, which will differ from their

relationships influenced by other rocks. Differing source rocks for marine sediments will not have differing influences only due to their mineral/chemical composition but also due to their varying susceptibility to weathering and other physico-chemical processes (Caridi et al., 2018; Radomirović et al., 2021). For example, granite, an igneous rock with high quartz content, will typically contain more uranium than limestones that are rich in calcite and poor in quartz (up to 15 ppm U in granites, 1–10 ppm U in limestones) (Runde and Neu, 2010). Additionally, calcite and dolomite are less resistant to weathering than amphiboles, biotite, K-feldspars, and muscovite (also comprising granite) and especially less resistant than quartz (Formoso, 2006). This will all be reflected in resulting sediments produced from the source rocks. Therefore, it is important to study MAR in all rock associations and resulting sediments that have not yet been studied or were poorly studied.

East Adriatic coast is typically karstic and is mostly built of carbonates. However, flysch deposits are also significantly present in Kaštela Bay coastal area (Fig. 1), which affects sedimentation in the Bay. Flysch zone in central Adriatic Sea extends from Kaštela Bay to the Neretva River mouth (Bogner and Matijević, 2016). Carbonates and flysch are untypical combination, but Kaštela Bay is a typical location representing it. Additionally, Kaštela Bay is one of such areas where anthropogenic activities (industry, transport, agriculture, tourism) were and still are intensive. These activities include chemical factory ("Adriavinil" or "Jugovinil", closed in 1990 after four decades of operation) and associated TENORM (fly and bottom ash) disposal on land and in the sea, cementworks, ironworks, electroplating facility, shipyard, shipworks, ports, recreational boating capacities, airport, high capacity greenhouses, brewery, and heavy traffic on the main road along the coast (Blanco et al., 2018; Lovrenčić Mikelić and Barišić, 2022b; Lovrenčić Mikelić et al., 2021; Rada et al., 2012; Ujević et al., 2010). Additionally, untreated industrial and municipal wastewaters were discharged into the Bay coupled with uncontrolled urban and agricultural runoff (Bogner and

Matijević, 2016; Lovrenčić Mikelić et al., 2017; Rada et al., 2012; Ujević et al., 2010). Anthropogenic activities made a significant impact on the area, especially in the second half of the 20th century (Bogner and Matijević, 2016; Lovrenčić Mikelić et al., 2022; Skoko et al., 2014). The whole area was strongly urbanised, industrialised, and polluted, with the peak in the 1980s (Bogner and Matijević, 2016; Miloš and Bensa, 2019; Ujević et al., 2010). Coastal area around the Bay is still highly urbanised, industrialised, and highly affected by anthropogenic activities, with the largest urban agglomeration on the east Adriatic Coast (Blanco et al., 2018; Lovrenčić Mikelić et al., 2021). The agglomeration comprised approx. 250,000 inhabitants in 2019 (Lovrenčić Mikelić and Barišić, 2022a). The situation with pollution improved in the 1990s and later (Bogner and Matijević, 2016; Rada et al., 2012; Ujević et al., 2010). However, the record of MAR in marine sediment remains (Bogner et al., 1998; Buljac et al., 2011; Kwokal et al., 2002; Mikac et al., 2006; Orescanin et al., 2005; Ujević et al., 2000, 1998). Therefore, it is important to know MAR's relationships and behaviour in these sediments. However, notwithstanding many conducted studies in Kaštela Bay, MAR have almost exclusively been researched separately and statistical clustering techniques have been applied only to terrestrial environment (Lovrenčić Mikelić et al., 2021, 2013). The researched metals were usually limited to a few typical heavy metals under strong anthropogenic influence, while studies on radionuclides were much rarer than on metals.

Kaštela Bay, as a typical carbonate-flysch coastal site with both natural and anthropogenic influences, was chosen for a study of MAR relationships in marine sediment using statistical clustering technique. The research objectives were to study: (i) relationships between five radionuclides (^{40}K, ^{226}Ra, ^{232}Th, ^{238}U, ^{137}Cs), 18 metals (Al, K, Ca, Ti, V, Cr, Mn, Fe, Co, Ni, Cu, Zn, Ga, Rb, Sr, Y, Pb, As), and sediment properties (organic matter, sediment grain size, and mineral composition); (ii) sediment sources; (iii) predominant influencing parameters on relationships. It is important to notice that distribution of MAR in

marine sediment is not in the scope of this study and it will be studied separately along with other relevant objectives.

2. Materials and Methods

2.1 Study Area

Kaštela Bay is located at the east coast of the central Adriatic Sea, adjacent to the city of Split, Croatia, (Fig. 1). It is a lens-shaped semi-enclosed bay defined by the mainland coast to the north, peninsula with the city of Split and Marjan hill to the southeast, and by the Čiovo Island to the southwest. It is one of the largest bays at the Croatian coast. Its total surface is approximately 60 km^2 and its maximum depth is 45–50 m at its entrance (Lovrenčić Mikelić et al., 2022). Morphologically, two distinct parts of the Bay are differentiated: shallow west part and deep/deeper central and east part. Surface streams around the Bay are scarce. The only permanent stream is the Jadro River in the easternmost part of the Bay. The coastal area is predominantly built of two types of rocks: Eocene varieties of flysch and flysch-like rocks and Cretaceous limestones and dolomites (Fig. 1). Other types are less represented and less important. More information on the Bay and its surroundings can be found in Lovrenčić Mikelić et al. (2022, 2021, 2017, 2013) and in Lovrenčić Mikelić and Barišić (2022a).

2.2 Sampling

Marine sediment was collected between June 2005 and May 2008 at 95 sampling stations (Fig. 1, Table 1). A regular grid of 1 × 1 km and 500 × 500 m around the Adriavinil factory was used for selection of stations. Samples were collected at three additional stations as well: KV01, KK, and KC. KV01 was selected due to vicinity of the Slatina submerged groundwater discharge, KK as a typical representative of fine grained sediments and higher sedimentation rate (approx. 0.4 cm/yr for 1954–2005, maximum: approx. 0.8 cm/yr for 1963–

2005/2006) in deep parts of the Bay, and KC as a typical representative of coarse grained sediments and lower sedimentation rate (approx. 0.1 cm/yr for 1954–2005, maximum: approx. 0.6 cm/yr for 1963–2005/2006) in shallow parts of the Bay (Lovrenčić Mikelić et al., 2017). Wherever possible, samples were collected by gravity corer. Three cores were taken at each station, with the exception of KK and KC stations. Otherwise, samples were collected by scuba diver with hand corer, when only one core was taken per station. The aim was to retrieve sediment cores of 50 cm length, but that was not always possible. Collected cores were sliced into segments in the field, placed into labelled plastic bags, and transported to laboratory. The segments were 5 cm wide from 0 cm to 30 cm depth and 10 cm wide from 30 cm to 50 cm depth. In total, 604 samples/segments were collected. Additional data referring to sampling are given in Lovrenčić Mikelić et al. (2022, 2017).

2.3 Gamma-Spectrometry

^{40}K, ^{226}Ra, ^{232}Th, ^{238}U, and ^{137}Cs massic activities were determined in all samples by gamma-spectrometry technique. Samples were first dried overnight at 105 °C, then ground, homogenised, placed into measuring containers (125 cm^3), weighed, sealed, and stored for at least four weeks to allow ingrowth of gaseous ^{222}Rn (Lovrenčić Mikelić and Barišić, 2022a).

HPGe detectors were used for analyses: coaxial with 25.3 % relative efficiency and InSpector 2000 with 25.4 % relative efficiency. Resolution at 1332.5 keV (^{60}Co) was 1.75 keV and 1.80 keV for coaxial and InSpector detectors, respectively. Detectors were coupled with multichannel analysers with 8192 channels (Canberra Industries). Spectra were collected for 80 000 s and analysed with Genie 2000 software package (Canberra Industries). All massic activities were recalculated to a reference date (6th June 2005). Detectors were protected with lead shielding in order to reduce the background radiation. InSpector 2000 was additionally protected with copper shielding.

^{40}K activity was determined through the 1460.75 keV peak, ^{226}Ra through 295.21 keV, 351.92 keV (^{214}Pb progeny), 609.31 keV, 1120.28 keV, and 1764.49 keV peaks (^{214}Bi progeny), ^{232}Th thorough 238.63 keV (^{212}Pb progeny), 338.32 keV, 911.20 keV, and 968.97 keV peaks (^{228}Ac progeny), ^{238}U through 63.29 keV and 92.6 keV peaks (^{234}Th progeny), and ^{137}Cs through the 661.66 keV peak. Interfering contributions to the 63.29 keV peak were subtracted. Background spectra were collected once in three months and subtracted from the subsequent experimental spectra.

Uncertainty budget comprised the following uncertainty sources: counting statistics of the peak area, gamma-ray emission probability, detector efficiency, and sample mass. The expanded uncertainty was expressed with $k = 2$ for $p = 95$ %. More details on sample preparation, gamma-spectrometry analysis, calibrations, and quality control are available in Lovrenčić Mikelić et al. (2022, 2021, 2017) and in Lovrenčić Mikelić and Barišić (2022a).

2.4 Energy Dispersive X-Ray Fluorescence

Al, K, Ca, Ti, V, Cr, Mn, Fe, Co, Ni, Cu, Zn, Ga, Rb, Sr, Y, Pb, and As mass fractions were determined in all samples by energy dispersive X-ray fluorescence technique. Samples were first dried at 105 °C to achieve constant mass, then ground to powder, homogenised, and prepared for analysis as thick targets. MiniPal 4 spectrometer (PANalytical, Almelo, Netherland) was used for analysis. All samples were measured in four sequences of 200 s each. Standard reference material IAEA-SL1 was used on a daily basis as a quality control sample and was measured as an unknown sample. Other details about the measurement conditions and the method are given in Lovrenčić Mikelić et al. (2013) and in references therein.

2.5 Determination of Organic Matter Mass Fractions

Organic matter (OM) mass fractions were determined in all samples. Samples were dried at 105 °C overnight, ground to powder, and homogenised. Then, they were weighed, heated for 12 hours at 375 °C, and weighed again. Mass fractions were determined from loss on ignition at 375 °C.

2.6 X-Ray Diffraction

Mineral composition was determined in eight samples from the KK (0–50 cm depth) and six samples from the KC (0–30 cm depth) sampling stations and in the K9005 sample (20–25 cm depth). These stations/samples were selected for analysis as the representative ones: the KK station for deep, fine-grained sediment, the KC station for shallow, coarse-grained sediment, and the K9005 sample for station under assumed strong anthropogenic influence. Only the K9005 sample was analysed from the K90 station because it was assumed that mineral composition will be the same in the first six segments and that the segment seven might be the Bay's natural sediment. This was based on visual inspection of the sediment core on-site and on the results of other analyses. The first six segments of the K90 sediment were unusually black. This was associated with the uncontrolled fly and bottom ash disposal into the sea close to the "Adriavinil" chemical factory. The ash was a by-product of coal combustion in the factory.

Samples were dried overnight at 105 °C, ground to powder, homogenised, placed into aluminium holders, and analysed with a Philips PW 1830 X-ray diffractometer with Cu tube, graphite crystal monochromator, and a proportional counter. Analyses were performed at room temperature. The current was 40 mA and the voltage 40 kV. Obtained data were processed by Philips X'Pert software. Relative intensities of X-ray diffraction lines were compared with the literature values (Orescanin et al., 2004).

2.7 Statistical Analysis

Statistical analyses were performed with Statistica 7.0 program package (StatSoft, Inc.). Measurement uncertainty was not taken into account in statistical analyses.

Outliers for radionuclides activities and metals and organic matter fractions were identified by scatter plots. The data from the remaining 587 samples, after excluded outliers, were used for correlation analysis. Pearson correlation coefficients were calculated for all radionuclides, all metals, and OM. Obtained values were statistically significant at $p < 0.05$.

Correlation analysis for radionuclides, metals, OM, and grain size was performed for 14 samples from the KK and the KC stations, because they were the only ones with available data on grain size. The data on grain size were previously published (Lovrenčić Mikelić et al., 2022, 2017). Hence, they were not presented in this study, but they were used for analysis. No outliers were found before the analysis. Pearson correlation coefficients were statistically significant at $p < 0.05$. Results of this analysis may be considered preliminary due to small number of samples. The output correlation matrix is truncated because correlations not related to grain size are given in the analysis of all samples.

Relationships between radionuclides, metals, and OM in eight studied sediment depths/layers were studied using PCA. The analysis was performed without excluding outliers, i.e. on all 604 samples, in order to better differentiate anthropogenic influence from other components. Maximum five principal components (or factors) were extracted but only components with eigenvalues greater than one were retained if they meaningfully explained the relationships between variables. Retained components were projected on factor-planes.

Selected variables (OM, Cu, Zn, Pb, Mn, As, ^{226}Ra, ^{238}U) were presented as scatter plots. Variables were selected based on the PCA results, i.e. variables having specific relationships or characteristics revealed by the PCA factors were selected.

Relationships found in marine sediments were compared with relationships in terrestrial rocks and sediments previously studied by multivariate statistical techniques (Lovrenčić Mikelić et al., 2021, 2013).

3. Results

3.1 Radionuclides Massic Activities, Metals and Organic Matter Mass Fractions

Basic statistical parameters for radionuclides massic activities, mass fractions of metals, and OM mass fractions are presented in Table 2. Generally, the highest activities of natural radionuclides are found for ^{40}K (according to mean value and median), although ^{226}Ra and ^{238}U show higher maxima. The lowest activities of natural radionuclides were found for ^{232}Th. ^{137}Cs activities are generally low, but they show its unambiguous presence in sediments. ^{226}Ra, ^{238}U, and ^{137}Cs activities maxima are significantly higher than their medians, approx. 35, 21, and 12 times, respectively. Ca, Al, Fe, K, and Ti are the most abundant metals, in the listed order. The most significant difference between maximum values and medians in metals was observed for Cu, Zn, and Pb, where the maxima were approx. 18, 43, and 80 times higher than the medians, respectively. OM maximum is also notably higher than its median, 6.7 times.

3.2 Mineral Composition

Results for mineral composition of sediments are presented in Table 3. Composition of samples from the KK and the KC sampling stations is not presented for each sample individually, but as a summary representation of the stations because diffraction spectra were identical for all samples of the respective stations.

Mineral composition of sediments at the KK and the KC stations is almost identical. Calcite and quartz are predominant at both stations. Quartz is a little less represented than

calcite. Halite, muscovite, and chlorite are subordinate to accessory at both stations. The only difference between the two stations is in the presence/absence of aragonite. Aragonite was determined only at the KC station. Halite was determined in all samples, although it is not a consequence of the sediment mineral composition, but of a seawater composition. Samples were oven dried during their preparation and halite from the water in wet sediment is retained in sediment after drying. Uniform mineral composition of sediments was observed in all segments of the KK and the KC stations.

Carbonate and silicate minerals predominate at the K90 station (i.e. in the K9005 sample), as it was found at the KK and the KC stations as well. Additionally, hematite and pyrite were found at the K90, which were not determined at other two stations. Carbonate minerals encompass calcite and Mg-calcite and silicates encompass quartz and illite/muscovite. Halite determined here also originates from the seawater. Mg-calcite and illite/muscovite are considerably abundant at the K90, while they were not present at all at the KK and the KC stations. Muscovite and chlorite were not determined at the K90 station, unlike at the KK and the KC.

3.3 Correlation Analysis

Seventeen outliers were found and excluded from correlation analysis of all samples. They were excluded because they were the most probably a result of the strong anthropogenic influence, which would mask natural influences. The whole K90 sampling station was excluded although the K9007 sample was not an outlier, but it was excluded for caution because a strong anthropogenic influence was expected at this station. OM, ^{226}Ra, ^{232}Th, ^{238}U, Ti, V, Fe, Co, and Y presented outliers at the K90. Outliers for Cr were found in K1801, for Mn and As in K2501–K2503, for Cu in K3203, and for Zn and/or Pb in K6101–K6105.

297 Results of the correlation analyses are given in Tables 4 and 5, for all stations/without grain
298 size and for KK and KC stations/with the grain size, respectively.
299 Almost all correlations in Table 4 were statistically significant. The exceptions were
300 the following pairs: Al–^{238}U/Zn/Pb, Sr–As, and Y–Zn/Pb/As. All five studied radionuclides
301 showed more or less statistically significant positive correlations with each other (r = 0.12–
302 0.95, Table 4). The lowest correlation was between ^{238}U and ^{137}Cs and the highest between
303 ^{40}K and ^{232}Th. Surprisingly, not so high correlation was observed between ^{226}Ra and ^{238}U (r =
304 0.57, Table 4). However, this was the highest correlation found for both radionuclides.
305 Generally, ^{137}Cs showed the lowest correlations with other radionuclides, followed by ^{238}U.
306 ^{40}K showed the highest correlations ($\geq$ |0.70|) with both other radionuclides and the majority
307 of metals. Very similar, although generally somewhat lower, correlations were observed
308 between ^{232}Th and other radionuclides and metals. ^{226}Ra and ^{238}U showed mostly weak
309 correlations with MAR. In fewer cases (four pairs for ^{226}Ra and seven pairs for ^{238}U), there
310 were no correlations or only slight correlations existed between these two radionuclides and
311 metals.
312 Among metals, only Ca and Sr were negatively correlated with all other MAR, while
313 their mutual correlation was positive and high or very high (r = 0.72, Table 4). Ca and Sr
314 correlations with all other variables were mostly high or very high, where Ca correlations
315 were generally higher than Sr correlations. Regarding correlations with radionuclides, Ca
316 presented the lowest correlations with ^{238}U (r = -0.23) and ^{226}Ra (r = -0.28) and the highest
317 with ^{40}K and ^{232}Th (r = -0.93 and r = -0.86, respectively) (Table 4). The same pattern was
318 observed for Sr correlations with radionuclides. Regarding Ca and Sr correlations with metals,
319 the lowest were found for Ca–Pb (r = -0.19) and for Sr–Pb (r = -0.25) and the highest were
320 for Ca–Ti/Fe (r = -0.95) and Sr–Ti (r = -0.78) (Table 4). Ca showed weak correlation at most
321 with Pb, Cu, Zn, Y, and As, while correlations with other metals were almost exclusively high

or very high. Similar, but somewhat lower, correlations were observed for Sr. Its correlations with Cu, Zn, and Pb were weak and with other metals they were real significant to high or very high.

Almost all metals, except Ca and Sr that are positively correlated only one to another, show mutual statistically significant positive correlations. The lowest correlation was observed for Al–As (r = 0.10) and the highest for Fe–Co (r = 0.98), followed by Fe–K/Ti (r = 0.97) and K–Ti and Rb–K/Ti/Fe (r = 0.96) (Table 4). The majority of metals' correlations (46 %) are high or very high. However, there is a significant fraction of weak/slight/non-existent correlations (39 %) related to Cu, Zn, Y, Pb, and As. Cu, Zn, Pb, and As show weak correlations at most with almost all other metals. Only Cu is an exception with its two real significant correlations (Cu–V: r = 0.42, Cu–Fe: r = 0.40) (Table 4). Y correlations are somewhat higher than those of Cu, Zn, Pb, and As, with more frequent real significant correlations (r = 0.40–0.51) (Table 4). It is observed that Cu, Zn, and Pb show high correlations (r = 0.78–0.83) only mutually, while they are low with other metals (Table 4). They also present real significant correlations (r = 0.46–0.51) with ^{137}Cs, while correlations with other radionuclides are lower.

Organic matter showed negative correlations only with Ca and Sr (r = -0.66 and r = -0.51, respectively) (Table 4). The majority of its correlations with radionuclides and metals are real significant (r = 0.40–0.67) (Table 4). The exceptions are OM–V (r = 0.73, high or very high) and OM–Y/As (r = 0.24 and r = 0.37, respectively, weak) (Table 4). Between radionuclides, the highest correlation was for OM–^{40}K (r = 0.64) followed by ^{137}Cs, ^{232}Th, ^{238}U, and ^{226}Ra (r = 0.40) (Table 4) in descending order.

Very high statistically significant correlations were observed between all granulometric fractions (r = 0.93–|1.00|) (Table 5). There is a distinct division to coarse- and fine-grained fractions.

Very high statistically significant correlations (r = |0.83|–|0.99|) (Table 5) exist between $^{40}K/^{226}Ra/^{232}Th/^{238}U$ and granulometric fractions. These four radionuclides show negative correlations with the coarse-grained fraction and positive with the fine-grained fraction. Only ^{137}Cs did not show any statistically significant correlations with granulometric fractions. However, it presents the same pattern as other radionuclides.

Almost all correlations between granulometric fractions and metals are statistically significant and high or very high (Table 5). The exceptions are: there are no statistically significant correlations of all granulometric fractions with Al and for As–GR, correlations for Pb–GR/CL and As–SA/SL/CL are lower (real significant). Only Ca and Sr show positive correlations with coarse-grained fractions and negative with fine-grained. The opposite pattern applies for other metals.

Correlations between OM and all granulometric fractions are statistically significant and very high (Table 5). OM is negatively correlated with the coarse-grained fraction and positively with the fine-grained.

3.4 Principal Component Analysis

Results of the PCA for radionuclides, metals, and OM in eight sediment depths/layers are presented in Figs. 2–9. The first four factors retained in sediment layers 1, 2, and 3 explained the following portions of cumulative variances: 86.3 %, 85.4 %, and 81.0 %, respectively (Figs. 2–4). The first three factors were retained in layers 4–8 and they explained cumulative variances in the following portions: layer 4 – 81.2%, layer 5 – 82.6 %, layer 6 – 85.2 %, layer 7 – 83.7 %, and layer 8 – 82.4 % (Figs. 5–9). Three groups of variables (G1–G3) are progressively differentiated with depth increase in all eight layers according to factors 1 and 2 (Figs. 2.a–9.a). The fourth group (G4) is differentiated only in the first three layers (0–15 cm depth) according to factor 4 (Figs. 2.c–4.c). Group 2 is further differentiated in two

372 subgroups (G2a and G2b) in all layers up to 40 cm depth according to factor 3 (Figs. 2.b–8.b).
373 In layer 8 at 40–50 cm depth, only G2a is present, while G2b is not (Fig. 9.b).
374 The most striking characteristic is a clear separation of Ca and Sr in G1 from all other
375 variables in all depths according to factor 1. Ca and Sr loadings on factor 2 are negligible in
376 all depths. They are very closely positioned on a factor-plane in all layers according to factors
377 1 and 2 and no significant changes were observed with depth changes. Loadings on factor 3
378 are negligible for both elements in all layers except in layer 8, where only Sr noticeable
379 positive loading on factor 3 was observed (Fig. 9.b). Sr has shown some loading on factor 4 in
380 the first two sediment layers, but not in the layer 3 (Figs. 2.c–4.c).
381 G2 and G3 are not always clearly differentiated from each other and some variables
382 are not always in the same group at different depths. G2 is differentiated according to
383 relatively high negative loadings on factor 2. Cu, Zn, and Pb are in this group in all layers
384 (Figs. 2.a–9.a). ^{238}U, ^{226}Ra, and OM are not in this group only in layer 8, where ^{238}U does not
385 show high loadings on any factor, while ^{226}Ra and OM are in G3 (Fig. 9.a). Arsenic and ^{137}Cs
386 were mostly in G2, with some deviations. Arsenic deviated closer to G1 in layer 3 (Fig. 4.a),
387 while it was in G3 in layer 8 (Fig. 9.a). ^{137}Cs was in G2 in layers 4–8 (Figs. 5.a–9.a), while in
388 the first three layers, it was in G3 (Figs. 2.a–4.a). It is observed that ^{137}Cs loadings on factor 2
389 become more negative with depth increase and that it increasingly separates ^{137}Cs from G3.
390 Vanadium is an example of transitional element between G2 and G3. It is closer to G2 in
391 layers 3–5 (Figs. 4.a–6.a), it is clearly in G3 in layers 7 and 8 (Figs. 8.a and 9.a), while it is
392 between G2 and G3 in other layers (Figs. 2.a, 3.a, and 7.a).
393 Differentiation of G2 into G2a and G2b is the clearest for Cu, Zn, and Pb that are in
394 the G2a in all sediment layers (Figs. 2.b–9.b). ^{137}Cs is in the G2a in layers 3–8 (Figs. 4.b–9.b),
395 while it is much closer to G1 in the first two layers (Figs. 2.b and 3.b). ^{226}Ra and ^{238}U are the
396 main constituents of G2b in which they show (very) close factor loadings. They are in this

subgroup in layers 1–7 (Figs. 2.b–8.b), while in layer 8 ^{238}U shows very high positive loading on factor 3 and ^{226}Ra moderate negative loading (Fig. 9.b). In layer 8, G2b does not exist and factor loadings associated with G2a are significantly lower than in other layers. It is interesting to note that OM was closely associated with ^{226}Ra in G2b only in layer 7 (Fig. 8.b), while it was closer to the majority of variables that would be in G3 in the factor-plane defined by factors 1 and 2.

G3 is differentiated by high negative loadings on factor 1 and low or moderate (mostly positive) loadings on factor 2 (Figs. 2.a–9.a). It comprises variables not encompassed by G1 and G2 on the factor-plane defined by factors 1 and 2. The majority of variables are in this group.

G4 differentiated by high negative (Fig. 2.c) or positive (Figs. 3.c and 4.c) loadings on factor 4 and it comprises only Mn and As. It is the only group differentiated by factor 4.

3.5 Scatter Plots

Scatter plots of Cu, Zn, Pb, Mn, As, ^{226}Ra, and ^{238}U vs. OM are presented in Fig. 10. Some locally elevated mass fractions and massic activities were observed. OM mass fractions were significantly elevated at the K90 sampling station (Figs. 10.a–g) and moderately elevated at the K60 and K61 (Figs. 10.a–c). Cu, Zn, and Pb fractions were elevated at the K61, while for Cu and Pb they were additionally elevated at the K21 and K60 (Figs. 10.a–c). Elevated Cu fraction was also found at the K32 station (Fig. 10.a). Both Mn and As mass fractions, were elevated at the K25, while elevated Mn fractions were also found at the K37 and K47 (Figs. 10.d–e). Elevated ^{226}Ra and ^{238}U massic activities were found at the K90 sampling station (Figs. 10.f–g).

4. Discussion

4.1 Differentiation of Sediment Sources

Mineral composition of sediment at the KK and KC stations points to mixed sediment sources, both carbonate and silicate. Abundance of Ca (from carbonates) and of Al, K, and Ti (from aluminosilicates) in all samples is in accordance with that (Table 2). Carbonate source is represented with calcite and aragonite, and silicate with quartz, muscovite, and chlorite (Table 3). Part of carbonate material is likely of terrigenous origin due to lithological composition of the Bay's surroundings, while other part is probably of biogenic origin. Predominant minerals in the coastal area were calcite (in limestones and marls) and quartz (in stream sediment and soils) (Lovrenčić Mikelić et al., 2013). Biogenic origin of material is supported by shells found in sediment and by determined aragonite. Aragonite was determined only at the KC station in the shallower part of the Bay, where shell fragments were found during sampling, suggesting aragonite's biogenic origin. This is in accordance with sedimentation energy conditions in different parts of the Bay. They were earlier discussed in Lovrenčić Mikelić et al. (2022, 2017). Skeletal fragments are coarse-grained and will be deposited in shallower, high-energy part of the Bay. Muscovite and chlorite imply weathering of the silicate rocks from the Bay's surroundings and deposition of terrestrial material in the Bay. It is supported by feldspars, chlorite, muscovite, and biotite determined in flysch deposits of the Bay's surroundings (Borović, 1999; Lovrenčić Mikelić et al., 2013). Muscovite was also determined in marls, stream sediments, and soils of the Kaštela Bay coastal area (Lovrenčić Mikelić et al., 2013). Spagnoli et al. (2008) stated that chlorite and illite are usually present in Adriatic sediments, although illite was not determined at the KK and KC stations. Uniform mineral composition of sediment observed in all layers at the KK and KC stations points to stable material input from the same source. Previous studies of Kaštela Bay found similar mineral composition supporting carbonate and silicate sediment sources. Orescanin et al. (2005) determined significant abundance of calcite and considerable

abundance of quartz in sediment. Muscovite, aragonite, and halite were also determined. Additionally, rhodochrosite, biotite, and siderite, which were not determined in the current study, were found. Bogner (1996) and Crmarić et al. (1999) also determined prevailing calcite and quartz in surficial sediments, accompanied by illite, feldspars, and aragonite in lesser amounts and associated with chlorite, dolomite, plagioclases, and K-feldspars.

Sediment at the K90 station, i.e. the K9005 sample, clearly shows different mineral composition compared to the KK and KC stations, pointing to different source of material at the K90. This is supported by significantly elevated OM fraction at the K90 compared to other sampling stations (Fig. 10) and by significantly increased ^{226}Ra and ^{238}U activities only at the K90 station (Figs. 10.f–g). Here, sediment most likely derives from two sources. One is rocks and sediments from the Bay's surroundings and the other is most likely associated with anthropogenic activities and disposing of bottom and fly ash into the sea. Fly and bottom ash as a source is in accordance with observed elevated ^{226}Ra and ^{238}U activities at the K90 station (Figs. 10.f–g). It is interesting that both hematite and pyrite were found in the same sample since they point to different redox conditions. Hematite is characteristic for oxidising conditions and pyrite for reducing. It is possible that hematite at the K90 station partly originates from *terra rossa* soil. Hematite is one of the most common pedogenic iron oxides in soils and, with goethite, is one of the most important pedogenic iron oxides in terra *rossa soils* (Durn, 2003; Durn et al., 2001). Lack of hematite at the KK and KC stations implies weak natural influence of the *terra rossa* soils on sediments and supports anthropogenic source of hematite at the K90. Another (more) possible source of hematite at the K90 are bottom and fly ash in which it is a by-product of coal combustion during which pyrite is oxidised in hematite (Liu et al., 2022; Waanders et al., 2003; Wei and Song, 2020). Hematite is regularly determined in coal combustion products and pyrite is one of the main iron bearing minerals in coals (Laita et al., 2019; Liu et al., 2022; Oliveira et al., 2011; Silva et al., 2011;

Spears et al., 1994; Waanders et al., 2003). Pyrite at the K90 most probably originates from its incomplete oxidation during coal combustion at lower temperatures (Waanders et al., 2003) since no evidence of pyrite in uncontaminated Kaštela Bay sediments was found. Another possibility is transformation of hematite into pyrite (reduction of Fe^{III} into Fe^{II}) in sediment in the presence of high OM content (Matijević et al., 2007; van de Velde et al., 2020). Elevated OM content (12–20 %) at the K90 was found earlier, compared to the rest of the Kaštela Bay sediments (mean value: 3.1 %, maximum: 5.6 %) (Lovrenčić Mikelić et al, 2022). It is also presented in Fig. 10. However, there is no sufficient data to support Fe^{III} reduction. Both, hematite and pyrite have not been earlier identified in sediments and rocks of the Bay's coastal area supporting their anthropogenic provenance in marine sediments (Lovrenčić Mikelić et al., 2013). Quartz, illite, and carbonates are also common in coal or its combustion by-products (Laita et al., 2019; Oliveira et al., 2011; Waanders et al., 2003; Wei and Song, 2020). Common carbonate minerals in coals are ankerite ($CaFe(CO_3)_2$) and siderite ($FeCO_3$) although dolomite and calcite may also be found (Waanders et al., 2003; Wei and Song, 2020). Due to their abundance at the KK and KC stations and in the rocks of the coastal area, it may be assumed that calcite and quartz at the K90 predominantly originate from surrounding rocks. On the other hand, magnesium calcite and illite/muscovite were found only at the K90 and with considerable abundance, pointing to fly or bottom ash as their source.

4.2 Relationships Between Radionuclides, Metals, Organic Matter, and Grain Size

Clear separation of Ca and Sr in G1 on a factor-plane (Figs. 2–9) in all sediment depths is attributed to their origin and/or geochemical behaviour, which are unchanged throughout the whole sediment profile. Ca and Sr are typical representatives of carbonate sediment component and are usually closely associated. This is in accordance with observed

correlations, where only Ca and Sr were negatively correlated with other MAR and grain size fractions (Tables 4 and 5). On the other hand, MAR in G3 represent the silicate component of sediment and are grouped with Al, K, and Ti that are typically incorporated in aluminosilicates and can be associated with the input of terrigenous material of non-carbonate origin (Liu et al., 2019; Lovrenčić Mikelić et al., 2021). It may be concluded that factor 1 in Figs. 2.a–9.a differentiates variables according to the most influencing sediment component (carbonate vs. silicate) and that it represents natural differences in geochemical behaviour of MAR. MAR in G3 will be preferentially bound to aluminosilicates, especially to clays, whose presence might be the most influential parameter affecting their behaviour since clays are very effective in adsorbing MAR (Liu et al., 2019; Novikau and Lujaniene, 2022).

Factor 2 (Figs. 2.a–9.a) is more complex and most probably represents both anthropogenic influence and partly possible natural processes of differentiation (e.g. preferential leaching or binding). They affect MAR and OM in G2, while those in G3 would not be affected. Consequently, MAR in G2 will not necessarily be preferably bound nor to carbonates neither to silicates, although they are more likely to be bound to silicates.

Among metals, Cu, Zn, and Pb show specific characteristics and should be discussed. Their close factor loadings (Figs. 2.b–9.b) suggest their same origin and occurrence in sediment. This is supported by their high or very high mutual correlations and poor correlations with all other metals and all radionuclides, except with ^{137}Cs (Table 4). Cu, Zn, Pb, and ^{137}Cs's common characteristic is their predominant or exclusive anthropogenic origin, although their sources differ. Another common characteristic might be the input pathway into marine sediment. They could have been deposited by atmospheric fallout (wet and dry), direct release into the sea, and/or terrestrial runoff as implied by their grouping in the G2a (Figs. 2.b–9.b). These pathways are not assumed for ^{226}Ra and ^{238}U since they are consistently separated in G2b (Figs. 2.b–9.b). All suggested input pathways are not equally important for

all four variables, depending on the source and environmental conditions. For example, Pb originating from leaded fuel may have been deposited directly by dry deposition on water surface and indirectly by runoff. Cu originating from vineyard soils due to long-term use of Cu-based fungicides would have been transported by runoff, while Cu from antifouling paints would have been deposited directly from water to marine sediment (Lagerström et al., 2020; Miloš and Bensa, 2019). Equally, Zn from traffic infrastructure would have been transported by runoff, while it would have been released into seawater from antifouling paints and then deposited in sediment. For ^{137}Cs, atmospheric fallout is expected to be the dominant pathway compared to terrestrial runoff, while there is no direct release into the sea. Relatively high or high Cu, Zn, and Pb correlations with OM and fine-grained sediment fraction (Tables 4 and 5) imply their preferred binding to fine particles. This is in accordance with the generally high adsorption capacity of fine-grained sediments for metals (Liu et al., 2019). Other metals, excluding Ca and Sr, also presented very similar correlations and the same pattern (Tables 4 and 5) showing that only Ca and Sr are preferably associated with coarse-grained fraction, while others are associated with fine-grained fraction (including OM). Very similar relationships between Cu, Zn, and Pb and between them and other metals and studied radionuclides were found earlier in Kaštela Bay coastal sediments and sedimentary rocks (Lovrenčić Mikelić et al., 2021, 2013). It was found that Cu, Zn, and Pb are most likely of anthropogenic origin or, less likely, that they represent a specific mineral assemblage. This suggests that the Cu, Zn, and Pb source for marine sediments are terrestrial rocks and sediments, partly or completely, or that both marine and terrestrial environments are influenced by the same source (e.g. urban and agricultural runoff or *terra rossa* soil) (Lovrenčić Mikelić et al., 2021). Anthropogenic source is supported by very high Cu, Zn, and Pb mass fractions maxima in sediments of the Bay (Table 2) compared with uncontaminated Kaštela Bay sediments in which the following fractions of the three metals were determined

(with the associated measurement uncertainty for p = 95 % and k = 2): Cu: (19.0±1.9) mg/kg, Zn: (71.9±3.7) mg/kg, Pb: (2.30±0.27) mg/kg (Lovrenčić Mikelić, 2011). This means that the maximum values for Cu, Zn, and Pb are 18, 50, and 70 times higher than in uncontaminated sediments, respectively. Anthropogenic source is also supported by elevated Cu, Zn, and Pb fractions observed locally (Figs. 10.a–c). Significant anthropogenic influence on Cu, Zn, and Pb in Kaštela Bay sediments was detected earlier by various authors (Bogner et al., 1997; Oreščanin et al., 2005; Ujević et al., 2000, 1998). Leaded fuel, car tyres, traffic infrastructure, extensive use of Cu-based fungicides in vineyards, cement plant, iron plant, bottom/fly ash deposit site, antifouling paints and coatings from shipyard and boat repairing facility, and electroplating facilities were specified as the sources of Cu, Zn, and/or Pb in sediments (Bogner et al., 2005, 1997; Miloš and Bensa, 2019; Oreščanin et al., 2005).

Additional variables that should be discussed are Mn and As, which are differentiated in G4, but only in the first three sediment layers (Figs. 2.c–4.c). The origin of differentiation is not immediately clear in terms of their source. They might both be of natural as well as of anthropogenic origin, at least partly. Some authors concluded that Mn in Kaštela Bay sediments originates from natural sources that include marl and *terra rossa* (Bogner, 1996; Bogner et al., 1998; Miko et al., 2003; Obhođaš et al., 2006; Ujević et al., 1998). However, locally elevated Mn and As fractions observed in Bay sediments (Figs. 10.d–e) might also be a consequence of pesticides and fertilizers use in agriculture (Biney et al., 1994; Gad, 2023; Sarkar and Datta, 2003). Since Mn and As are clearly separated from Cu, Pb, and Zn, as typical anthropogenic metals, according to factors 3 and 4 (Figs. 2.b–9.b, 2.c–4.c), it may be assumed that anthropogenic influence on Mn and As is much weaker than on Cu, Pb, and Zn and that Mn and As have a different source compared to these three metals. This is supported by low correlation coefficients between Mn–Cu/Zn/Pb and As–Cu/Zn/Pb, where they were in 0.14–0.26 and 0.32–0.34 ranges, respectively (Table 4). Separate source of Mn and As is also

supported by Fig. 10, where Mn and As show elevated values at different sampling stations (K25, K37, and/or K47; Figs. 1 and 10.d–e) compared to Cu, Pb, and Zn that showed elevated values at the opposite part of the Kaštela Bay (K21, K32, K60, and/or K61; Figs. 1 and 10.a–c). If they would all have the same source, it would be expected for all of these metals to be accumulated and to present elevated values in the same area, which is not the case here. Finally, it may be assumed that Mn and As are differentiated in G4 due to predominantly natural sources possibly mixed with anthropogenic sources, unlike Cu, Pb, and Zn that were differentiated due to predominantly anthropogenic sources.

^{226}Ra and ^{238}U show relationships similar to Cu, Zn, and Pb although they are not always very close to the three metals on the factor-plane defined by factors 1 and 2 (Fig. 2.a–9.a). It should be noted that similar relationships pattern does not automatically represent any kind of dependence between the two radionuclides and three metals. On the contrary, no/slight/weak correlations observed between these radionuclides and metals (Table 4) do not imply any dependency between them. Therefore, ^{226}Ra and ^{238}U behaviour should be considered separately. This is supported by clear separation of ^{226}Ra and ^{238}U in G2b according to factor 3, while Cu, Pb, and Zn are in G2a (Figs. 2.b–9.b). Unlike Cu, Zn, Pb, and ^{137}Cs, ^{226}Ra and ^{238}U may be associated with direct disposal of TENORM into the sea, which is supported by elevated ^{226}Ra and ^{238}U values at the K90 sampling station (Figs. 10.f–g). In layers 1–6, ^{226}Ra and ^{238}U have almost identical factor loadings on the factor-plane (Figs. 2.b–7.b), which points to their same geochemical behaviour and occurrence in sediment and/or the same source. However, they start to differentiate subtly in layer 7 (Fig. 8.b), while they are completely uncoupled in layer 8 (Fig. 9.b). The situation in layer 8 might be attributed to changed mobility of ^{226}Ra and/or ^{238}U. It may be assumed that the dominant process here is preferential ^{238}U leaching from sediment enhanced by the presence of Ca, while ^{226}Ra becomes preferably bound to silicates and less mobile. Greater influence of natural processes

on ^{226}Ra and ^{238}U behaviour than of a possible anthropogenic origin in deeper sediment layers is supported by high or relatively high factor loadings of ^{238}U and ^{226}Ra and by low factor loadings of Cu, Zn, Pb, and ^{137}Cs as variables under strong or exclusive anthropogenic impact (Fig. 9.b). Similar ^{226}Ra–^{238}U relationship was observed in Kaštela Bay coastal unconsolidated sediments, where it was discussed in more detail (Lovrenčić Mikelić et al., 2021). Relatively low correlation between ^{226}Ra and ^{238}U (Table 4) supports the possibility of different natural processes affecting them and causing their different geochemical behaviour in marine sediment. However, this possibility needs to be further studied. Poor ^{226}Ra and ^{238}U correlations with all MAR and their only real significant correlation with OM (Table 4), coupled with the PCA results (Figs. 2.a–9.a, Fig. 8.b), suggest that ^{226}Ra and ^{238}U behaviour and distribution might be associated with OM to some extent and that they are mostly not preferably bound to any of the MAR. High correlations of ^{226}Ra and ^{238}U with grain size fractions (Table 5) point to their preferred binding to fine-grained particles as found earlier (Dowdall and O'Dea, 1999; Shetty et al., 2006).

On the other hand, ^{40}K and ^{232}Th showed almost the opposite behaviour. Their very high mutual correlation (Table 4) and a constant grouping in G3 (Figs. 2.a–9.a) point to their identical geochemical behaviour and/or sources. They are preferably associated with terrestrial particles and aluminosilicates. These include clay minerals and the fine-grained sediment fraction in general, as suggested by their very high correlations with silt and clay fractions (Table 5). It was also previously shown that ^{40}K and ^{232}Th are preferably bound to fine-grained fraction (Powel et al., 2007; van der Graaf et al., 2007). The same behaviour of ^{40}K and ^{232}Th was observed in both consolidated rocks and sediments of Kaštela Bay coastal area (Lovrenčić Mikelić et al., 2021). Additionally, ^{40}K and ^{232}Th's mostly high or very high correlations with studied metals (Table 4), unlike for ^{226}Ra and ^{238}U, also support their association with aluminosilicates and aluminosilicate-bound metals, these being all metals in

622 G3 (Figs. 2.a–9.a). Both, ^{40}K and ^{232}Th presented higher correlations with OM than ^{226}Ra and
623 ^{238}U (Table 4), suggesting that OM might be more important for ^{40}K and ^{232}Th binding than
624 for ^{226}Ra and ^{238}U.

625 Dominant processes influencing ^{137}Cs differ at different sediment depths. ^{137}Cs
626 dependency on the input of terrigenous material and preferred binding to silicates, primarily
627 clay minerals, are more pronounced in upper sediment layers (1–3), where it is found in G3
628 (Figs. 2.a–4.a). Starting from layer 4, it is progressively closer to G2 that is characterised by
629 strong anthropogenic influence, while the importance of terrigenous material and silicates
630 diminishes (Figs. 5.a–9.a). Higher ^{137}Cs massic activities in Kaštela Bay marine sediments
631 were generally found in upper sediment layers reflecting anthropogenic impact (Lovrenčić
632 Mikelić et al., 2022, 2017). However, this is not reflected in layers 1–3 in Figs. 2.a–4.a. These
633 higher activities might themselves be the explanation for ^{137}Cs relationships in layers 1–3.
634 More ^{137}Cs in sediment makes it more competitive for binding to clay minerals and its affinity
635 for clays is the dominant parameter. As its activity diminishes with the increase of depth, it is
636 less competitive and its affinity for clays is not as emphasised as it is its anthropogenic origin.
637 Although ^{137}Cs correlations with grain size fractions were not statistically significant (Table
638 5), a pattern may still be observed, showing its possible preferential binding to silt and clay.
639 ^{137}Cs in marine systems is primarily bound to fine-grained sediments and is strongly adsorbed
640 to clay particles (Bobos et al., 2021; Figueira et al., 2006; Park et al., 2004). Lower ^{137}Cs
641 correlations with grain size fractions might be attributed to sediment mineral composition.
642 Namely, none of the minerals determined in sediment at the KK and KC stations has a high
643 adsorption affinity for ^{137}Cs (Kim et al., 2007). Only muscovite might have somewhat higher
644 ^{137}Cs adsorption affinity due to its crystallographic structure, which is similar to biotite
645 structure that is important in ^{137}Cs adsorption (Kim et al., 2007). Generally similar ^{137}Cs
646 relationships were observed in stream sediments and soils of Kaštela Bay coastal area

(Lovrenčić Mikelić et al., 2021), where predominant parameters for ^{137}Cs distribution were its anthropogenic origin and the introduction path in sediments. Introduction path is not completely differentiated in marine sediments because ^{137}Cs is in the same group with Cu, Zn, and Pb (Figs. 4.b–9.b), which in not the case in terrestrial sediments. However, low correlations of ^{137}Cs with other radionuclides (Table 4) may point to both its different (anthropogenic) origin and input path into sediment (atmospheric fallout) (Bobos et al., 2021). The highest correlations of ^{137}Cs with Cu, Zn, and Pb (except OM) are in accordance with their anthropogenic origin, although they derive from different sources. ^{137}Cs preferential binding to aluminosilicates was not the predominant parameter in terrestrial sediments, while in marine sediments this was a clear case only in deeper sediment layers (6–8) (Figs. 7.a–9.a). Some differences between marine and terrestrial sediments may be attributed to their genesis that affects their homogenisation and relationships between MAR and other variables. Stream sediments and soils are more homogenised and of a lesser thickness than marine sediments in which the thickness of the sediment column may play an important role.

Due to OM in G2 in layers 1–7 (Figs. 2.a–8.a), it may be assumed that at least some portion of it may be of anthropogenic origin in these layers, while it is not likely in layer 8 (Fig. 9.a). It is supported by the difference between median/mean value and maximum for OM (Table 2), which implies some locally elevated mass fractions of OM. Maximum OM value, originating from the K9007 sample (Fig. 10), is reflected in layer 7, where OM is grouped with ^{226}Ra and ^{238}U (Fig. 8.b). The same situation was observed for As (Figs. 2.a–8.a, Table 2), except that it has not shown the deviation in layer 7 as OM has (Fig. 8.b). Arsenic was better differentiated with Mn in G4 and it was earlier discussed with it. Elevated OM content may be associated with a former discharge of large quantities of untreated industrial and municipal wastewater or with other anthropogenic activities (Bogner et al., 1998; Ujević et al., 1998). According to correlations in Table 5, OM is associated with fine-grained

672 sediment fraction, as expected, and as it was found by other authors (Matijević et al., 2008;
673 Vdović and Juračić, 1993). However, this is clearly visible only in sediment layer 8 (Fig. 9.a).
674 It is attributed to strong anthropogenic influence in layers 1–7 that masks the natural
675 association of OM with fine-grained particles, including clays (i.e. aluminosilicates in G3
676 (Figs. 2.a–8.a)). Anthropogenic influence on OM in layer 8 is expected to be significantly
677 diminished and its natural affinity for aluminosilicates is shown (Fig. 9.a).
678
679 ***4.3 Environmental Considerations***
680 Radionuclides (primarily ^{226}Ra, ^{238}U, ^{137}Cs) and metals (primarily Cu, Zn, Pb) that
681 might be or are under anthropogenic influence may present adverse effects on sediment
682 quality and human health due to their radioactivity and/or toxicity and possible local
683 accumulation in sediment. MAR accumulated in sediments (even if only locally elevated)
684 may be latter redistributed to sediments of the larger area thus influencing initially
685 uncontaminated or less contaminated sediments. In the case of radionuclides, attention should
686 also be given to radiological risks.
687 The presence of pyrite and the pyrite/hematite stability at the K90 station should also
688 be addressed from the environmental point of view. Pyrite tends to bind an array of trace
689 elements, potentially toxic, but by its oxidation, these elements are released in environment
690 and may have toxic impact (Silva et al., 2011; Spears et al., 1994). Oxidation or dissolution of
691 pyrite easily lead to acidic conditions and acidification of natural waters, which may influence
692 the stability of other minerals (e.g. solubility increase) (Silva et al., 2011; Waanders et al.,
693 2003). This is enhanced by microbial activity and elevated OM content. On the other hand,
694 reduction of hematite may also occur and serve as a source of potentially toxic, previously
695 hematite bound, elements, since pyrite acts as a source of reductants for oxidised species (Liu
696 et al., 2019; Silva et al., 2011). This is especially possible under anoxic conditions.

Some studies suggest the possibility of simultaneous stability of pyrite and hematite in the same sediment with bistability redox conditions occurring in modern coastal marine sediments, which seem to be susceptible to bistability (van de Velde et al., 2020). These conditions are governed by iron, sulphur, and OM supply. The existence of possible Fe/S bistability in sediment renders pyrite/hematite relationship even more complex.

4.4 Study Limitations

Larger set of data for grain size analysis would be beneficial in order to obtain more reliable correlations of grain size with other researched variables. More data on mineral composition from selected stations would enable more detailed view of mixed carbonate-silicate sedimentation. It would reveal parts of the Bay where silicate input is increased. It would also be useful in identifying other stations with possible strong anthropogenic interventions (deposition of material into the sea). Redox conditions at the station influenced by deposition of fly and bottom ash may only be assumed at this moment and it would be recommended to study them more closely in order to determine any adverse effect if present. It is advised to further study the relationship between hematite and pyrite and their stability in sediment. Since this study clearly indicated anthropogenic impact on researched sediment, it would be recommended to further study MAR of interest and OM in terms of their distribution and sources. The current study could only suggest general sources, but not all specific sources could have been determined.

5. Conclusions

Sediments may be differentiated according to exposure to anthropogenic activities based on their mineral composition. However, this can be clearly performed only when foreign material has been deposited alongside the natural sediment. Differentiation of

sediment sources is not always unambiguous in cases of mixed natural and anthropogenic sources. Both, natural (carbonate and aluminosilicate rocks and sediments) and anthropogenic (fly and bottom ash) sediment sources were identified in Kaštela Bay. Predominantly carbonate sedimentation is influenced by input of aluminosilicates.

MAR showing specific characteristics in both marine and terrestrial sediments were primarily Cu, Zn, Pb, and ^{137}Cs, followed by ^{226}Ra and ^{238}U. Strong anthropogenic influence on Cu, Zn, Pb, and ^{137}Cs was found in both types of sediments. Anthropogenic impact on ^{226}Ra and ^{238}U was also visible, but they were probably additionally influenced by natural processes of separation, unlike ^{40}K and ^{232}Th. Mn and As showed specific characteristics only in marine sediments.

Relationships between MAR and sediment properties in marine sediment are more complex than in coastal terrestrial sediments. Predominant influencing parameters change with depth in marine sediment. This was observed for ^{226}Ra, ^{238}U, ^{137}Cs, and OM. In shallower sediment layers, ^{226}Ra, ^{238}U, and OM were predominantly under anthropogenic influence, while natural processes were predominant in the deepest sediment. Although ^{137}Cs is only of anthropogenic provenance, significant influence of natural processes was observed in shallower sediment, while its anthropogenic origin became more emphasised in deeper sediment. Unlike in coastal stream sediments and soils, ^{137}Cs in marine sediments was not differentiated from other variables under strong anthropogenic impact according to their origin and introduction path into environment.

Majority of MAR in marine sediment showed clear and consistent preferential association with aluminosilicates at all sediment depths. This association was less clear or less consistent for Cu, Zn, Pb, As, V, ^{226}Ra, ^{238}U, ^{137}Cs, and OM. None of the MAR and OM showed preferential association with carbonates.

Funding Source Disclosure

The research was funded by the Ministry of Science, Education, and Sports of the Republic of Croatia (grant number 098-0982934-2713, “Radionuclides and trace elements in environmental systems” project). Financial support from the Kaštela town was received for part of sampling. The funding sources had no involvement in study design, in the collection, analysis and interpretation of data, in the writing of the manuscript, and in the decision to submit the article for publication.

Acknowledgements

The authors would like to thank the crew of the research vessel “Hidra” of the Hydrographic Institute in Split for their assistance in sampling.

References

Aközcan, S., Uğur Görgün, A., 2013. Trace metal and radionuclide pollution in marine sediments of the Aegean Sea (Izmir Bay and Didim). Environ. Earth Sci. 69, 2351-2355.

Álvarez-Iglesias, P., Rubio, B., 2009. Geochemistry of marine sediments from inner Ría de Vigo (NW Spain). J. Radioanal. Nucl. Chem. 281, 247-251.

Aziman, E. S., Ismail, A. F., Jubri, S. F., Rahmat, M. A., Idris, W. M. R., 2021. Environmental impact assessment of post illegal mining activities in Chini Lake with regards to natural radionuclides and heavy metals in water and sediment. J. Radioanal. Nucl. Chem. 330, 667-683.

Biney, C., Amuzu, A. T., Calamari, D., Kaba, N., Mbome, I. L., Naeve, H., Ochumba, P. B. O., Osibanjo, O., Radegonde, V., Saad, M. A. H., 1994. Review of Heavy Metals, in: Calamari, D., Naeve. H., (Eds.), Review of Pollution in the African Aquatic Environment. CIFA Technical Paper No. 25, FAO, Rome, pp. 33-60.

772 Blanco, M., Pérez-Albaladejo, E., Piña, B., Kušpilić, G., Milun, V., Lille-Langøy, R.,
773 Karlsen, O. A., Goksøyr, A., Porte, C. 2018. Assessing the environmental quality of
774 sediments from Split coastal area (Croatia) with a battery of cell-based bioassays. Sci. Tot.
775 Environ. 624, 1640-1648.
776 Bobos, I., Madruga, M. J., Reis, M., Esteves, J., Guimarães, V., 2021. Clay mineralogy
777 insights and assessment of the natural (^{228}Ra, ^{226}Ra, ^{210}Pb, ^{40}K) and anthropogenic (^{137}Cs)
778 radionuclides dispersion in the estuarine and lagoon systems along the Atlantic coast of
779 Portugal. Catena. 206, 105532.
780 Bogner, D., Juracic, M., Odžak, N., Baric, A., 1998. Trace metals in fine grained sediments of
781 the Kaštela Bay, Adriatic Sea. Water Sci. Technol. 38(11), 169-175.
782 Bogner, D., Matijević, A., 2016. Variety of physical-chemical characteristics of Holocene
783 sediments from the middle Adriatic Sea (Croatia). Acta Adriat. 57(1), 3-16.
784 Bogner, D., Ujević, I., Barić, A., 2005. Trace metal (Cd, Pb, Cu, Zn and Cr) distribution in
785 sediments along east coast of the Adriatic Sea (Croatia). Fresenius Environ. Bull. 14(1), 50-
786 58.
787 Bogner, D., 1996. Superficial sediments and impact of their physico–chemical properties on
788 the distribution of heavy metals in the Kastela Bay (in Croatian). Ms. Sc. thesis, Faculty of
789 Science, Zagreb.
790 Borović, I., 1999. Geology of the Kaštela area (in Croatian), in: Hodžić, M. (Ed.),
791 Proceedings Kaštela kolijevka Hrvatske. Matica hrvatska Kaštela, Kaštela, pp. 183-188.
792 Buljac, M., Bogner, D., Cerjan-Stefanovic, S., Bolanca, T., Margeta, K., 2011. Cr and Zn
793 distribution in sediment from the semi-enclosed Kastela Bay, the Adriatic Sea (Croatia).
794 Fresenius Environ. Bull. 20, 853-860.
795 Caridi, F., Messina, M., Faggio, G., Santangelo, S., Messina, G., Belmusto, G., 2018.
796 Radioactivity, radiological risk and metal pollution assessment in marine sediments from

797 Calabrian selected areas, southern Italy. Eur. Phys. J. Plus. 133, 65.
798 https://doi.org/10.1140/epjp/i2018-11887-1.
799 Crmarić, R., Bogner, D., Juračić, M., 1999. Holocene sediments and sedimentation in Kaštela
800 Bay (in Croatian), in: Hodžić, M. (Ed.), Proceedings Kaštela kolijevka Hrvatske. Matica
801 hrvatska Kaštela, Kaštela, pp. 178-182.
802 Dowdall, M., O'Dea, J., 1999. Speciation of ^{226}Ra, ^{238}U and ^{228}Ra in an Upland Organic Soil
803 Overlying a Uraniferous Granite. Radiochim. Acta. 87, 109-114.
804 Durn, G., 2003. Terra Rossa in the Mediterranean Region: Parent Materials, Composition and
805 Origin. Geol. Croat. 56(1), 83-100.
806 Durn, G., Slovenec, D., Čović, M., 2001. Distribution of Iron and Manganese in Terra Rossa
807 from Istria and its Genetic Implications. Geol. Croat. 54(1), 27-36.
808 Feng, H., Cochran, J. K., Hirschberg, D. J., Wilson, R. E., 1998. Small-Scale Spatial
809 Variations of Natural Radionuclide and Trace Metal Distributions in Sediments From the
810 Hudson River Estuary. Estuaries, 21(2), 263-280.
811 Figueira, R. C. L., Tessler, M. G., de Mahiques, M. M., Cunha, I. I. L., 2006. Distribution of
812 ^{137}Cs, ^{238}Pu and $^{239+240}$Pu in sediments of the southeastern Brazilian shelf-SW Atlantic
813 margin. Sci. Total Environ. 357, 146-159.
814 Formoso, M.L.L., 2006. Some topics on geochemistry of weathering: a review. An. Acad.
815 Bras. Cienc. 78(4), 809-820.
816 Fouskas, F., Godelitsas, A., Argyraki, A., Pappa, F. K., Tsabaris, C., 2018. Metal
817 concentrations and radioactivity in sediments at the northern coastal zone of Ikaria Island,
818 eastern Mediterranean, Greece. J. Radioanal. Nucl. Chem. 317, 55-68.
819 Gad, S. C., 2023. Manganese, in: Reference Module in Biomedical Sciences, Elsevier,
820 https://doi.org/10.1016/B978-0-12-824315-2.00629-1.

Kim, Y., Kim, K., Kang, H.-D., Kim, W., Doh, S.-H., Kim, D.-S., Kim, B.-K., 2007. The accumulation of radiocesium in coarse marine sediment: Effects of mineralogy and organic matter. Mar. Pollut. Bull. 54, 1341-1350.

Külahcı, F., Şen, Z., 2008. Multivariate statistical analyses of artificial radionuclides and heavy metals contaminations in deep mud of Keban Dam Lake, Turkey. Appl. Radiat. Isot. 66, 236-246.

Kwokal, Ž., Frančišković-Bilinski, S., Bilinski, H., Branica, M., 2002. A comparison of anthropognic mercury pollution in Kaštela Bay (Croatia) with pristine estuaries in Öre (Sweden) and Krka (Croatia). Mar. Pollut. Bull. 44, 1152-1169.

Lagerström, M., Ytreberg, Wiklund, A.-K. E., Granhag, L., 2020. Antifouling paints leach copper in excess – study of metal release rates and efficacy along a salinity gradient. Wat. Res. 186, 116383. https://doi.org/10.1016/j.watres.2020.116383.

Laita, E., Bauluz, B., Yuste, A., 2019. High-temperature mineral phases generated in natural clinkers by spontaneous combustion of coal. Minerals. 9(4), 213. https://doi.org/10.3390/min9040213.

Liu, B., Zhang, W., Chi, G., 2019. Distribution and Risk Assessment of Heavy Metals in Sediment from Bohai Bay, China. Minerals. 9, 111. doi:10.3390/min9020111.

Liu, J., Peng, A., Deng, S., Liu, M., Liu, G., Li, C., 2021. Distribution of heavy metals and radionuclides in the sediments and their environmental impacts in Nansha Sea area, South China Sea. Mar. Pollut. Bull. 166, 112192.

Liu, L., Liu, Q., Zhang, S., Li, Y., Yang, L., 2022. The thermal transformation behavior and products of pyrite during coal gangue combustion. Fuel. 324(C), 124803. https://doi.org/10.1016/j.fuel.2022.124803.

844 Lovrenčić Mikelić, I., Barišić, D., 2022a. Radiological risks from ^{40}K, ^{226}Ra and ^{232}Th in
845 urbanised and industrialised karstic coastal area (Kaštela Bay, Croatia). Environ. Sci. Pollut.
846 Res. 29, 54632-54640.
847 Lovrenčić Mikelić, I., Barišić, D., 2022b. Natural and anthropogenic radionuclides in karstic
848 coastal area (Kaštela Bay, Adriatic Sea, Croatia) exposed to anthropogenic activities:
849 distribution, sources, and influencing factors. Radiochim. Acta. https://doi.org/10.1515/ract-
850 2022-0045.
851 Lovrenčić Mikelić, I., Cukrov, N., Oreščanin, V., Škaro, K., Barišić, D., 2022. ^{137}Cs Sediment
852 Profiles as a Tracer of Marine Sedimentation Processes in a Semi-Enclosed Bay Affected by
853 Anthropogenic Releases – Example of Kaštela Bay (Adratic Sea, Croatia). Water. 14, 2655.
854 Lovrenčić Mikelić, I., Oreščanin, V., Barišić, D., 2013. Distribution and origin of major,
855 minor, and trace elements in sediments and sedimentary rocks of the Kaštela Bay (Croatia)
856 coastal area. J. Geochem. Explor. 128, 1–13.
857 Lovrenčić Mikelić, I., Oreščanin, V., Barišić, D., 2021. ^{40}K, ^{226}Ra, ^{232}Th, ^{238}U and ^{137}Cs
858 relationships and behaviour in sedimentary rocks and sediments of a karstic coastal area
859 (Kaštela Bay, Croatia) and related rocks and sediments' differentiation. Environ. Sci. Pollut.
860 Res. 28, 51497-51510.
861 Lovrenčić Mikelić, I., Oreščanin, V., Škaro, K., 2017. Variation of sedimentation rate in the
862 semi-enclosed bay determined by ^{137}Cs distribution in sediment (Kaštela Bay, Croatia). J.
863 Environ. Radioact. 166, 112–125.
864 Lovrenčić Mikelić, I., 2011. Radionuclides, metals and arsenic in the Kaštela Bay sediments
865 (in Croatian). Ph.D. thesis, Faculty of Science, Zagreb.
866 Matijević, S., Bogner, D., Morović, M., Tičina, V., Grbec, B., 2008. Characteristics of the
867 sediment along the eastern Adriatic coast (Croatia). Fresenius Environ. Bull. 17(10b), 1763-
868 1772.

869 Matijević, S., Kušpilić, G., Kljaković-Gašpić, Z., 2007. The redox potential of sediment from
870 the Middle Adriatic region. Acta Adriat. 48(2), 191-204.
871 Mikac, N., Foucher, D., Kwokal, Ž., Barišić, D., 2006. Mercury and Radionuclides in
872 Sediments of the Kaštela Bay (Croatia) – Evaluation of the Sediment Pollution History. Croat.
873 Chem. Acta 79(1), 85-93.
874 Miko, S., Durn, G., Adamcová, R., Čović, M., Dubíková, M., Skalský, R., Kapelj, S., Ottner,
875 F., 2003. Heavy metal distribution in karst soils from Croatia and Slovakia. Environ. Geol. 45,
876 262-272.
877 Miloš, B., Bensa, A., 2019. Cd, Cu, Pb and Zn in terraced soil on flysch deposits of Kaštela
878 Bay coastal area, Croatia. J. Cent. Eur. Agric. 20(3), 974-985.
879 Novikau, R., Lujaniene, G., 2022. Adsorption behaviour of pollutants: Heavy metals,
880 radionuclides, organic pollutants, on clays and their minerals (raw, modified and treated): A
881 review. J. Environ. Manage. 309, 114685. https://doi.org/10.1016/j.jenvman.2022.114685.
882 Obhođaš, J., Kutle, A., Valković, V., 2006. Concentrations of some elements in the coastal sea
883 sediments: Bays with marinas. J. Radioanal. Nucl. Chem. 270(1), 75-85.
884 Oliveira, M., Waanders, F. B., Silva, L., Jasper, A., Sampaio, C., Dursman, M., Rachel, S.,
885 Hower, J., 2011. A Multi-analytical approach to understand the chemistry of Fe-minerals in
886 feed coals and ashes. Coal Combust. Gasif. Prod. 3(1), 51-62.
887 Orescanin, V., Barisic, D., Mikelic, L., Lovrencic, I., Rubcic, M., Rozmaric-Macefat, M.,
888 Lulic, S., 2004. Environmental Contamination Assessment of the Surroundings of the ex-
889 Šibenik's Ferro-manganese Smelter, Croatia. J. Environ. Sci. Health. A39(9), 2493-2506.
890 Orescanin, V., Barisic, D., Lovrencic, I., Mikelic, L., Rozmaric-Macefat, M., Pavlovic, G.,
891 Lulic, S., 2005. The influence of fly and bottom ash deposition on the quality of Kastela Bay
892 sediments. Environ. Geol. 49, 53-64.

Park, G., Lin, X. J., Kim, W., Kang, H. D., Lee, H. L., Kim, Y., Doh, S. H., Kim, D. S., Yun, S. G., Kim, C. K., 2004. Properties of ^{137}Cs in marine sediments off Yangam, Korea. J. Environ. Radioact. 77, 285-299.

Powell, B. A., Hughes, L. D., Soreefan, A. M., Falta, D., Wall, M., De Vol, T. A., 2007. Elevated concentrations of primordial radionuclides in sediments from the Reedy River and surrounding creeks in Simpsonville, South Carolina. J. Environ. Radioact. 94, 121-128.

Rada, B., Santic, M., Kupresanin, M., 2012. Monitoring DNA Damage in *Mytilus galloprovincialis* from the Kastela Bay in Croatia. Russ. J. Ecol. 43(1), 77-81.

Radomirović, M., Stanković, S., Mandić, M., Jović, M., Janković Mandić, Lj., Dragović, S., Onjia, A., 2021. Spatial distribution, radiological risk assessment and positive matrix factorization of gamma-emitting radionuclides in the sediment of the Boka Kotorska Bay. Mar. Pollut. Bull. 169, 112491. https://doi.org/10.1016/j.marpolbul.2021.112491.

Runde, W., Neu, M.P., 2010. Actinides in the geosphere, in: Morss, L.R., Edelstein, N.M., Fuger, J. (Eds.), The chemistry of the actinide and transactinide elements. Springer, Dordrecht, pp. 3475–3593.

Sarkar, D., Datta, R., 2003. A modified in-vitro method to assess bioavailable arsenic in pesticide-applied soils. Environ. Pollut. 126(3), 363-366.

Sauvé, D., Clulow, V., Goulet, R. R., 2021. Quantifying historical releases and pre-operation levels of metals and radionuclides. J. Environ. Radioact. 237, 106683.

Shahrokhi, A., Adelikhah, M., Chalupnik, S., Kovács, T., 2021. Multivariate statistical approach on distribution of natural and anthropogenic radionuclides and associated radiation indices along the north-western coastline of Aegean Sea, Greece. Mar. Pollut. Bull. 163, 112009.

Shetty, P. K., Narayana, Y., Siddappa, K., 2006. Vertical profiles and enrichment pattern of natural radionuclides in monazite areas of coastal Kerala. J. Environ. Radioact. 86, 132-142.

Silva, L. F. O., Macias, F., Oliveira, M. L. S., Kátia da Boit, M., Waanders, F., 2011. Coal cleaning residues and Fe-minerals implications. Environ. Monit. Assess. 172, 367-378.

Skoko, B., Marović, G., Babić, D., 2014. Radioactivity in the Mediterranean flora of the Kaštela Bay, Croatia. J. Environ. Radioact. 135, 36-43.

Spagnoli, F., Bartholini, G., Dinelli, E., Giordano, P., 2008. Geochemistry and particle size of surface sediments of Gulf of Manfredonia (Southern Adriatic Sea). Estuar. Coast. Shelf Sci. 80, 21-30.

Spears, D. A., Martinez Tarazona, M. R., Lee, S., 1994. Pyrite in UK coals: its environmental significance. Fuel. 73(7), 1051-1055.

Suresh, G., Ramasamy, V., Meenakshisundaram, V., Venkatachalapathy, R., Ponnusamy, V., 2011. Influence ofmineralogical and heavy metal composition on natural radionuclide concentrations in the river sediments. Appl. Radiat. Isot. 69, 1466-1474.

Topcuoğlu, S., Ergül, H. A., Baysal, A., Ölmez, E., Kut, D., 2003. Determination of radionuclide and heavy metal concentrations in biota and sediment samples from Pazar and Rize stations in the eastern Black Sea. Fresenius Environ. Bull. 12(7), 695-699.

Ujević, I., Kljaković-Gašpić, Z., Bogner, D., 2010. Influence of suspended matter on cadmium accumulation in sediment from Kaštela Bay, Adriatic Sea, Croatia. Acta Adriat. 51(1), 79-88.

Ujević, I., Odžak, N., Barić, A., 1998. Relationship between Mn, Cr, Pb and Cd concentrations, granulometric composition and organic matter content in the marine sediments from a contaminated coastal area. Fresenius Environ. Bull. 7, 183-189.

Ujević, I., Odžak, N., Barić, A., 2000. Trace metal accumulation in different grain size fractions of the sediments from a semi-enclosed bay heavily contaminated by urban and industrial wastewaters. Water Res. 34(11), 3055-3061.

van der Graaf, E. R., Koomans, R. L., Limburg, J., de Vries, K., 2007. In situ radiometric mapping as a proxy of sediment contamination: Assessment of the underlying geochemical and physical principles. Appl. Radiat. Isot. 65, 619-633.

van de Velde, S. J., Reinhard, C. T., Ridgwell, A., Meysman, F. J. R., 2020. Bistability in the redox chemistry of sediments and oceans. Proc. Natl. Acad. Sci. U.S.A. 117(52), 33043-33050.

Vdović, N., Juračić, M., 1993. Sedimentological and Surface Characteristics of the Northern and Central Adriatic Sediments. Geol. Croat. 46(1), 157-163.

Waanders, F. B., Vinken, E., Mans, A., Mulaba-Bafubiandi, A. F., 2003. Iron minerals in coal, weathered coal and coal-ash – SEM and Mössbauer results. Hyperfine Interact. 148/149, 21-29.

Wanjeri, V. W. O., Okuku, E. O., Barsanti, M., Schirone, A., Delbono, I., Owato, G., 2021. Baseline radionuclide and heavy metal concentrations in sediments of Sabaki River estuary (Kenya, Indian Ocean). Mar. Pollut. Bull. 164, 112033.

Wei, Q., Song, W., 2020. Mineralogical and chemical characteristics of coal ashes from two high-sulfur coal-fired power plants in Wuhai, Inner Mongolia, China. Minerals. 10, 323. https://doi:10.3390/min10040323.

Figure captions

Fig. 1. Location of Kaštela Bay, sampling stations, and simplified lithological map of the area (after Lovrenčić Mikelić et al., 2017, 2013).

Fig. 2. PCA of radionuclides massic activities, metals mass fractions, and organic matter mass fractions in sediment of Kaštela Bay at 0–5 cm depth (layer 1): **a)** Projection of factor 1 vs. factor 2; **b)** Projection of factor 1 vs. factor 3; **c)** Projection of factor 1 vs. factor 4; G – group. Rounded rectangles and rounded rectangular callouts explain poorly visible labels.

Fig. 3. PCA of radionuclides massic activities, metals mass fractions, and organic matter mass fractions in sediment of Kaštela Bay at 5–10 cm depth (layer 2): **a)** Projection of factor 1 vs. factor 2; **b)** Projection of factor 1 vs. factor 3; **c)** Projection of factor 1 vs. factor 4; G – group. Rounded rectangles and rounded rectangular callouts explain poorly visible labels.

Fig. 4. PCA of radionuclides massic activities, metals mass fractions, and organic matter mass fractions in sediment of Kaštela Bay at 10–15 cm depth (layer 3): **a)** Projection of factor 1 vs. factor 2; **b)** Projection of factor 1 vs. factor 3; **c)** Projection of factor 1 vs. factor 4; G – group. Rounded rectangles and rounded rectangular callouts explain poorly visible labels.

Fig. 5. PCA of radionuclides massic activities, metals mass fractions, and organic matter mass fractions in sediment of Kaštela Bay at 15–20 cm depth (layer 4): **a)** Projection of factor 1 vs. factor 2; **b)** Projection of factor 1 vs. factor 3; G – group. Rounded rectangles and rounded rectangular callouts explain poorly visible labels.

Fig. 6. PCA of radionuclides massic activities, metals mass fractions, and organic matter mass fractions in sediment of Kaštela Bay at 20–25 cm depth (layer 5): **a)** Projection of factor 1 vs. factor 2; **b)** Projection of factor 1 vs. factor 3; G – group. Rounded rectangles and rounded rectangular callouts explain poorly visible labels.

Fig. 7. PCA of radionuclides massic activities, metals mass fractions, and organic matter mass fractions in sediment of Kaštela Bay at 25–30 cm depth (layer 6): **a)** Projection of factor 1 vs. factor 2; **b)** Projection of factor 1 vs. factor 3; G – group. Rounded rectangles and rounded rectangular callouts explain poorly visible labels.

Fig. 8. PCA of radionuclides massic activities, metals mass fractions, and organic matter mass fractions in sediment of Kaštela Bay at 30–40 cm depth (layer 7): **a)** Projection of factor 1 vs. factor 2; **b)** Projection of factor 1 vs. factor 3; G – group. Rounded rectangles and rounded rectangular callouts explain poorly visible labels.

Fig. 9. PCA of radionuclides massic activities, metals mass fractions, and organic matter mass fractions in sediment of Kaštela Bay at 40–50 cm depth (layer 8): **a)** Projection of factor 1 vs. factor 2; **b)** Projection of factor 1 vs. factor 3; G – group. Rounded rectangles and rounded rectangular callouts explain poorly visible labels.

Fig. 10. Scatter plots of selected variables vs. organic matter (OM): **a)** Cu–OM; **b)** Zn–OM; **c)** Pb–OM; **d)** Mn–OM; **e)** As–OM; **f)** ^{226}Ra–OM; **g)** ^{238}U–OM.

Figure 1.

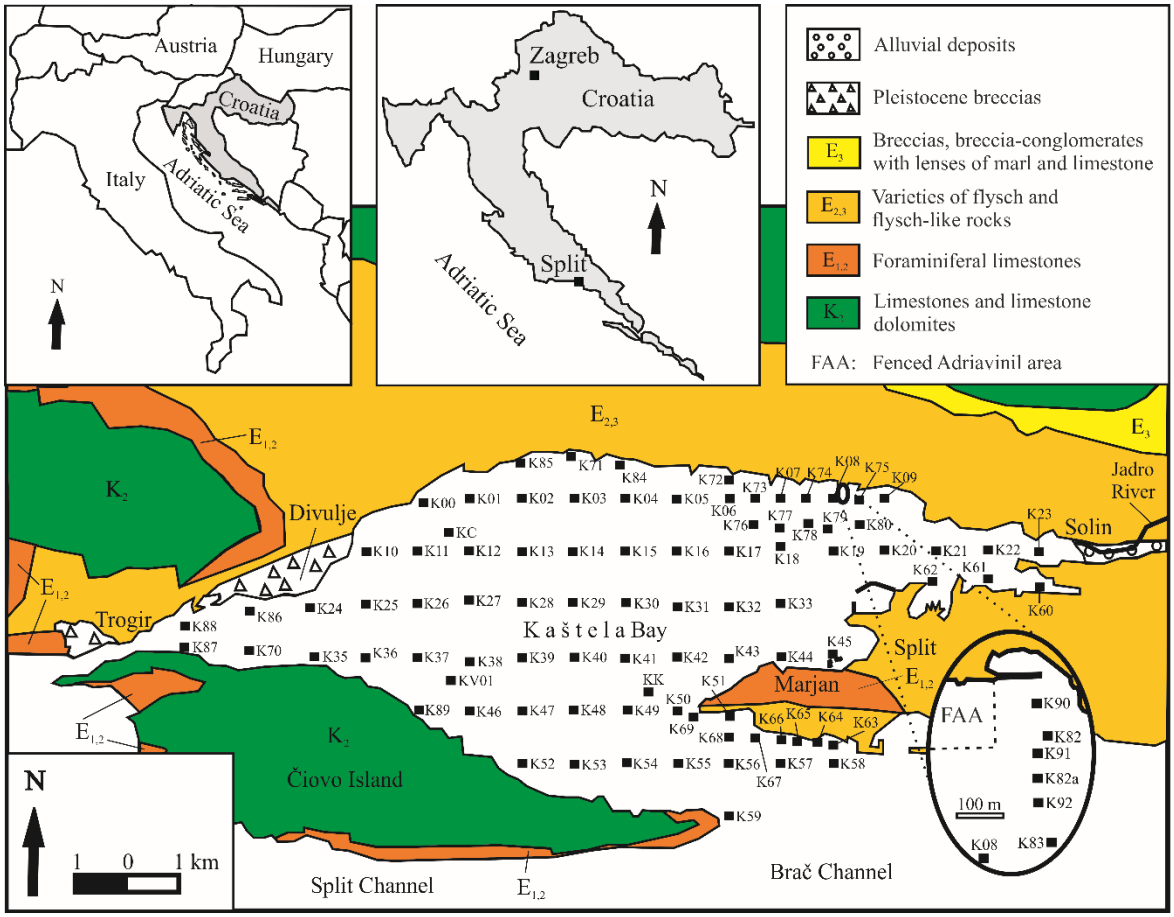
Austria
Hungary
Croatia
Italy
Adriatic Sea
N
Zagreb
Croatia
N
Split
Adriatic Sea
Alluvial deposits
Pleistocene breccias
E3 Breccias, breccia-conglomerates with lenses of marl and limestone
E2,3 Varieties of flysch and flysch-like rocks
E1,2 Foraminiferal limestones
K2 Limestones and limestone dolomites
FAA: Fenced Adriavinil area
E2,3
E3
E1,2
K2
Divulje
Jadro River
Solin
Trogir
Kaštela Bay
Split
Marjan
FAA
Čiovo Island
Split Channel
Brač Channel
100 m
N
1 0 1 km

Figure 2.

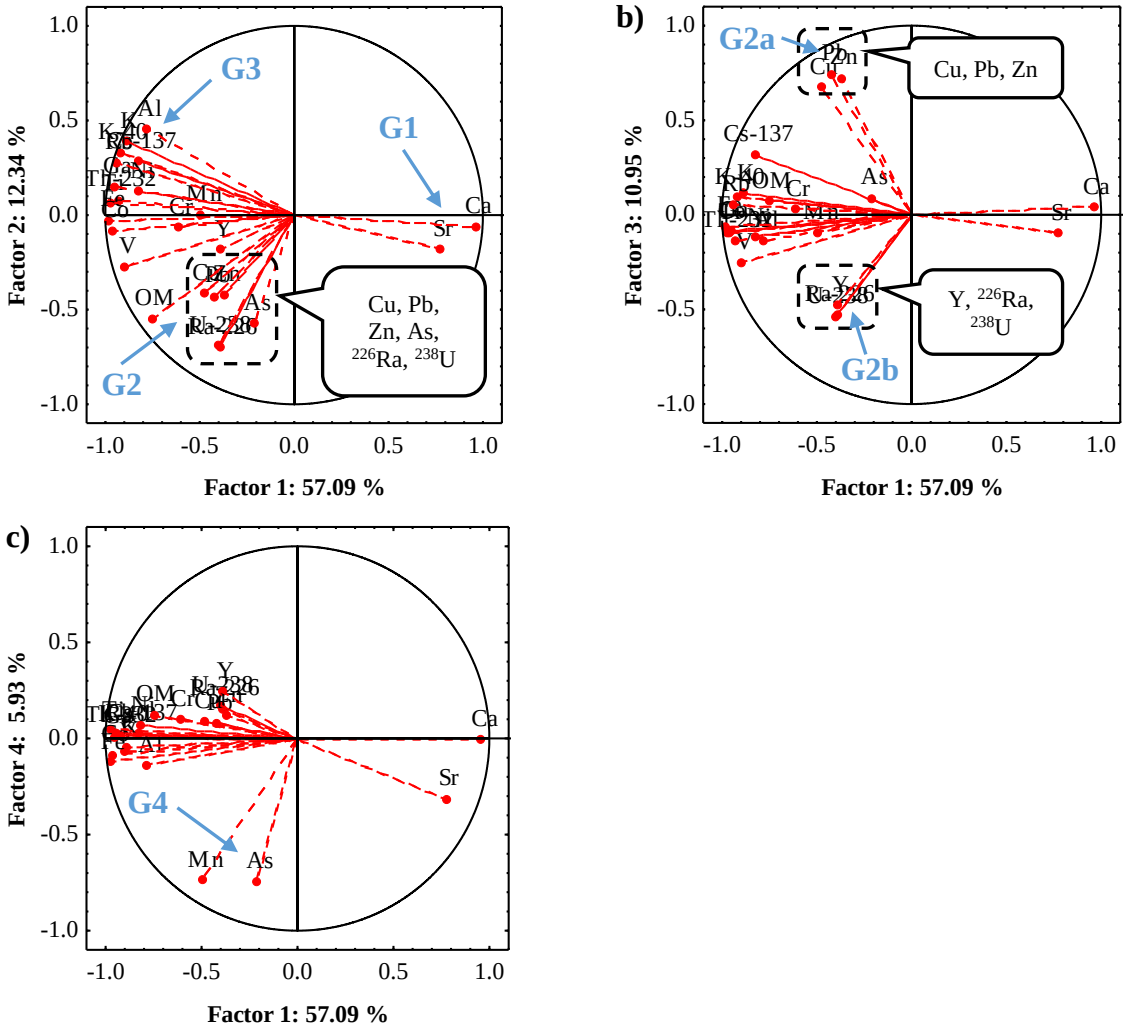
b)
c)
G1
G2
G2a
G2b
G3
G4
Cu, Pb, Zn
Cu, Pb, Zn, As, 226Ra, 238U
Y, 226Ra, 238U
Factor 1: 57.09 %
Factor 2: 12.34 %
Factor 3: 10.95 %
Factor 4: 5.93 %
Ca
Sr
As
Mn
OM
Cs-137
Al
V
Y
1.0
0.5
0.0
-0.5
-1.0

Figure 3.

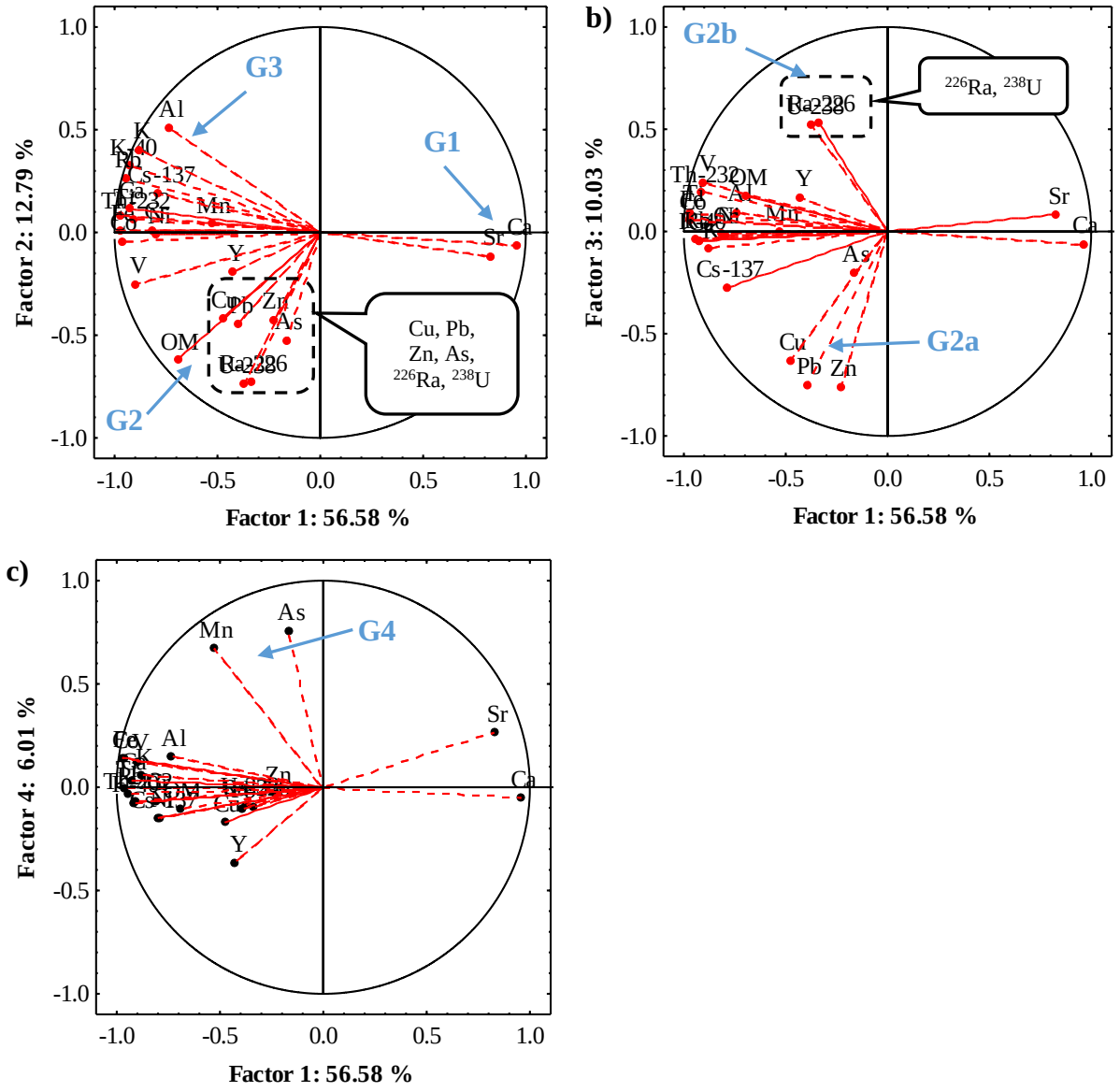
G3
G1
G2
Al
K
K-40
Cs-137
Mn
Ni
Co
V
Y
Cu
Pb
Zn
As
OM
Ra-226
Sr
Ca
Cu, Pb, Zn, As, 226Ra, 238U
Factor 2: 12.79 %
Factor 1: 56.58 %
b)
G2b
G2a
226Ra, 238U
Th-232
Sr
Ca
Cs-137
As
Cu
Pb
Zn
Factor 3: 10.03 %
Factor 1: 56.58 %
c)
G4
Mn
As
Sr
Ca
Al
Y
Factor 4: 6.01 %
Factor 1: 56.58 %

Figure 4.

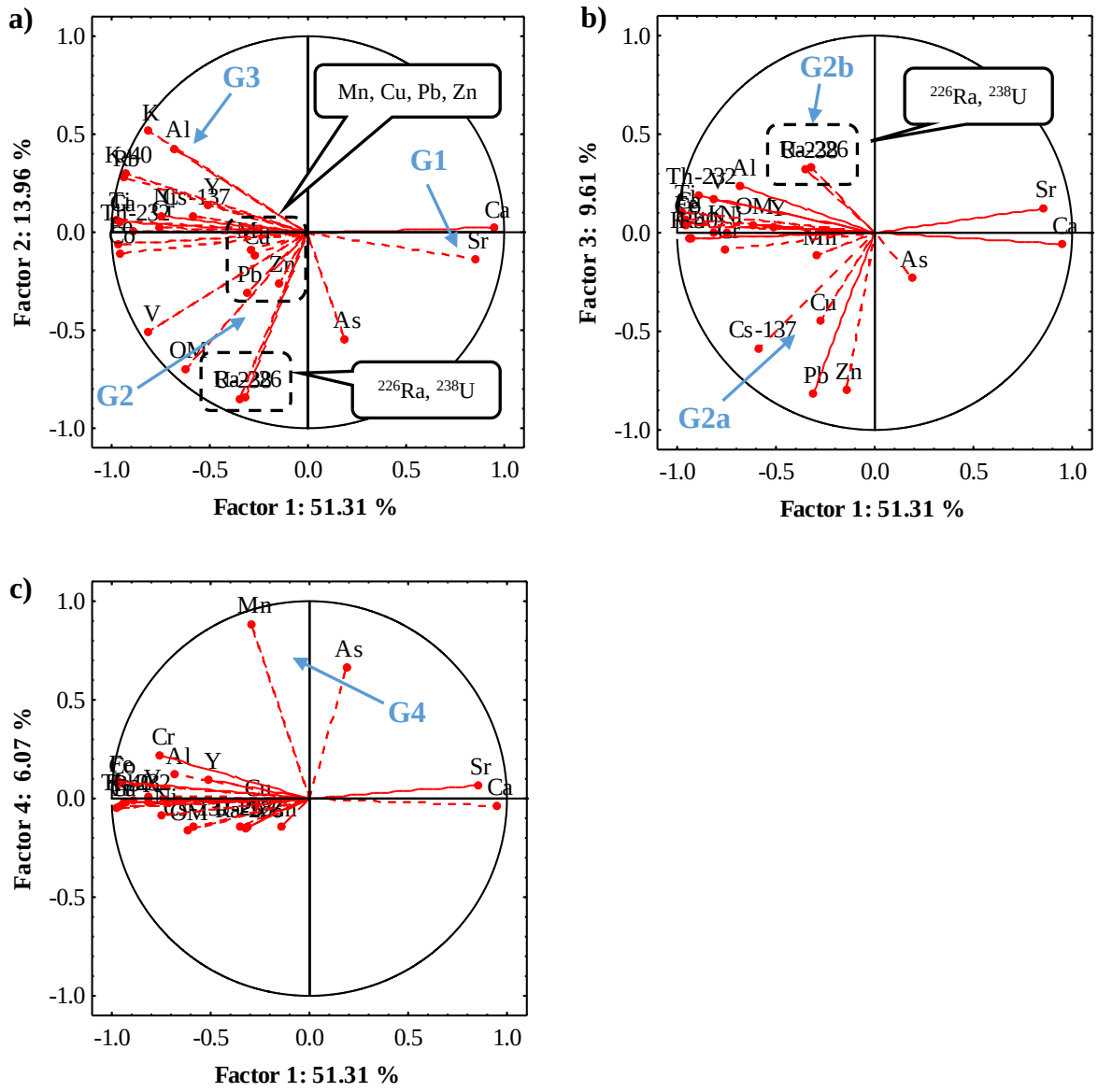
a)
G3
Mn, Cu, Pb, Zn
G1
G2
226Ra, 238U
Factor 2: 13.96 %
Factor 1: 51.31 %
b)
G2b
226Ra, 238U
G2a
Factor 3: 9.61 %
Factor 1: 51.31 %
c)
G4
Factor 4: 6.07 %
Factor 1: 51.31 %

Figure 5.

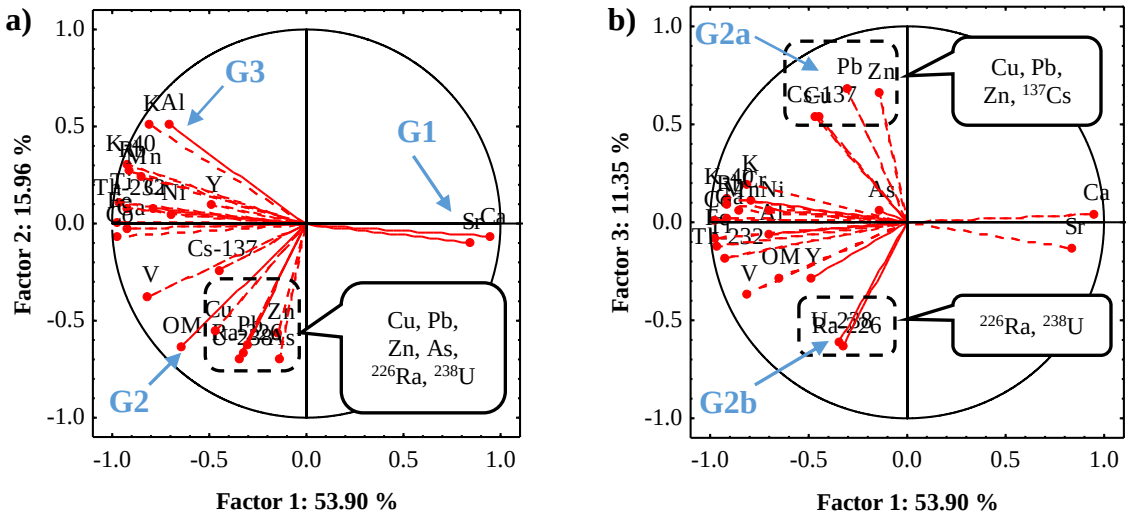
a)
G3
G1
G2
Cu, Pb, Zn, As, 226Ra, 238U
Cs-137
V
Sr
Ca
Factor 2: 15.96 %
Factor 1: 53.90 %
b)
G2a
G2b
Cu, Pb, Zn, 137Cs
226Ra, 238U
Pb
Zn
Cu
Ca
Sr
V
OM
Y
Factor 3: 11.35 %
Factor 1: 53.90 %

Figure 6.

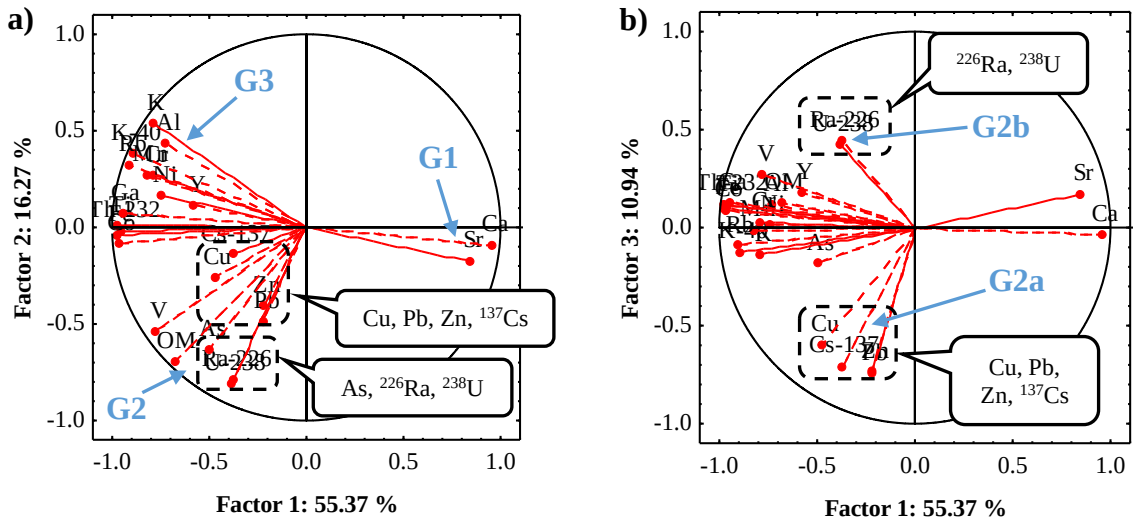
a)
G3
G1
G2
Cu, Pb, Zn, 137Cs
As, 226Ra, 238U
Factor 2: 16.27 %
Factor 1: 55.37 %
b)
226Ra, 238U
G2b
G2a
Cu, Pb, Zn, 137Cs
Factor 3: 10.94 %
Factor 1: 55.37 %

Figure 7.

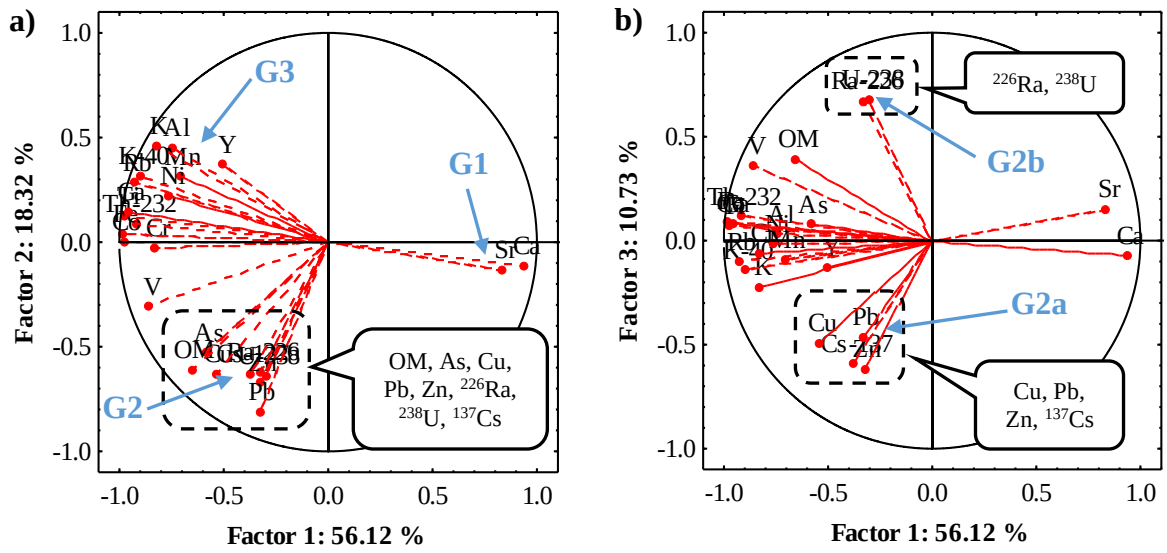
a)
G3
G1
G2
OM, As, Cu, Pb, Zn, 226Ra, 238U, 137Cs
Factor 2: 18.32 %
Factor 1: 56.12 %
b)
226Ra, 238U
G2b
G2a
Cu, Pb, Zn, 137Cs
Factor 3: 10.73 %
Factor 1: 56.12 %

Figure 8.

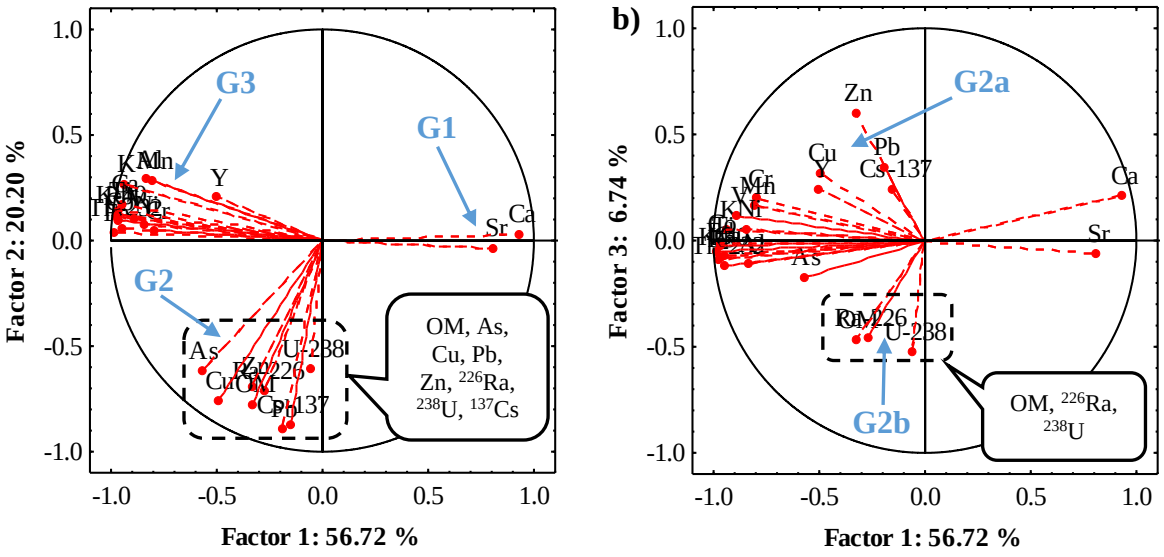
b)
G3
G1
G2
G2a
G2b
Y
Sr
Ca
As
Zn
Cu
Pb
Cs-137
U-238
OM, As, Cu, Pb, Zn, 226Ra, 238U, 137Cs
OM, 226Ra, 238U
Factor 2: 20.20 %
Factor 1: 56.72 %
Factor 3: 6.74 %
Factor 1: 56.72 %

Figure 9.

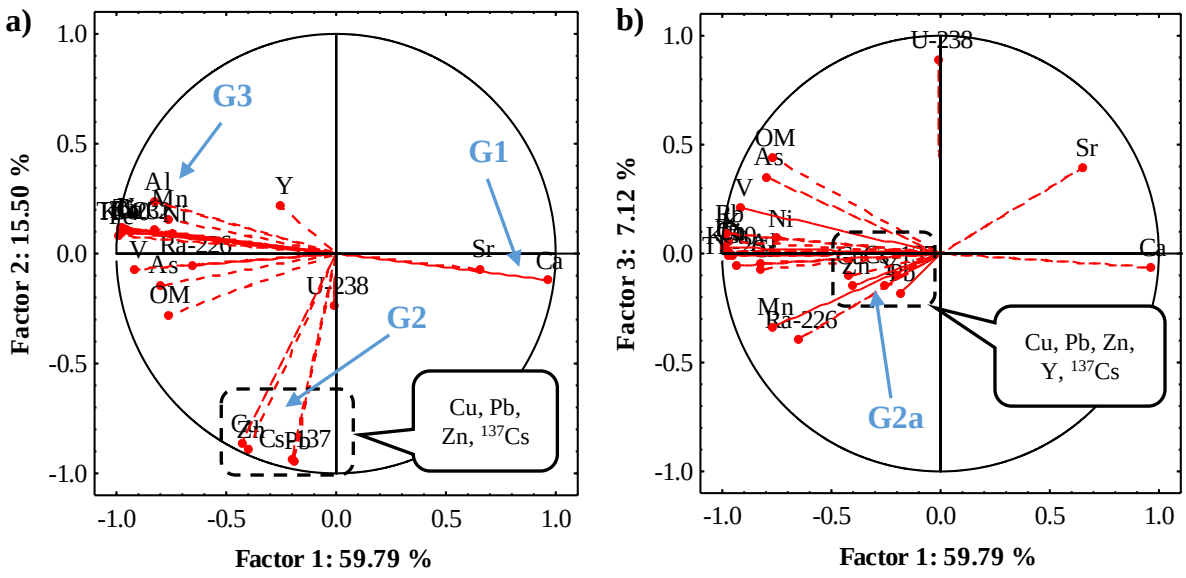
a)
G3
G1
G2
Y
Al
Mn
Ni
V
Ra-226
As
OM
Sr
Ca
U-238
Zn
Cs
Pb
137
Cu, Pb,
Zn, 137Cs
Factor 2: 15.50 %
Factor 1: 59.79 %
b)
U-238
OM
As
V
Ni
Sr
Ca
Mn
Ra-226
Zn
Pb
Cu, Pb, Zn,
Y, 137Cs
G2a
Factor 3: 7.12 %
Factor 1: 59.79 %

Figure 10.

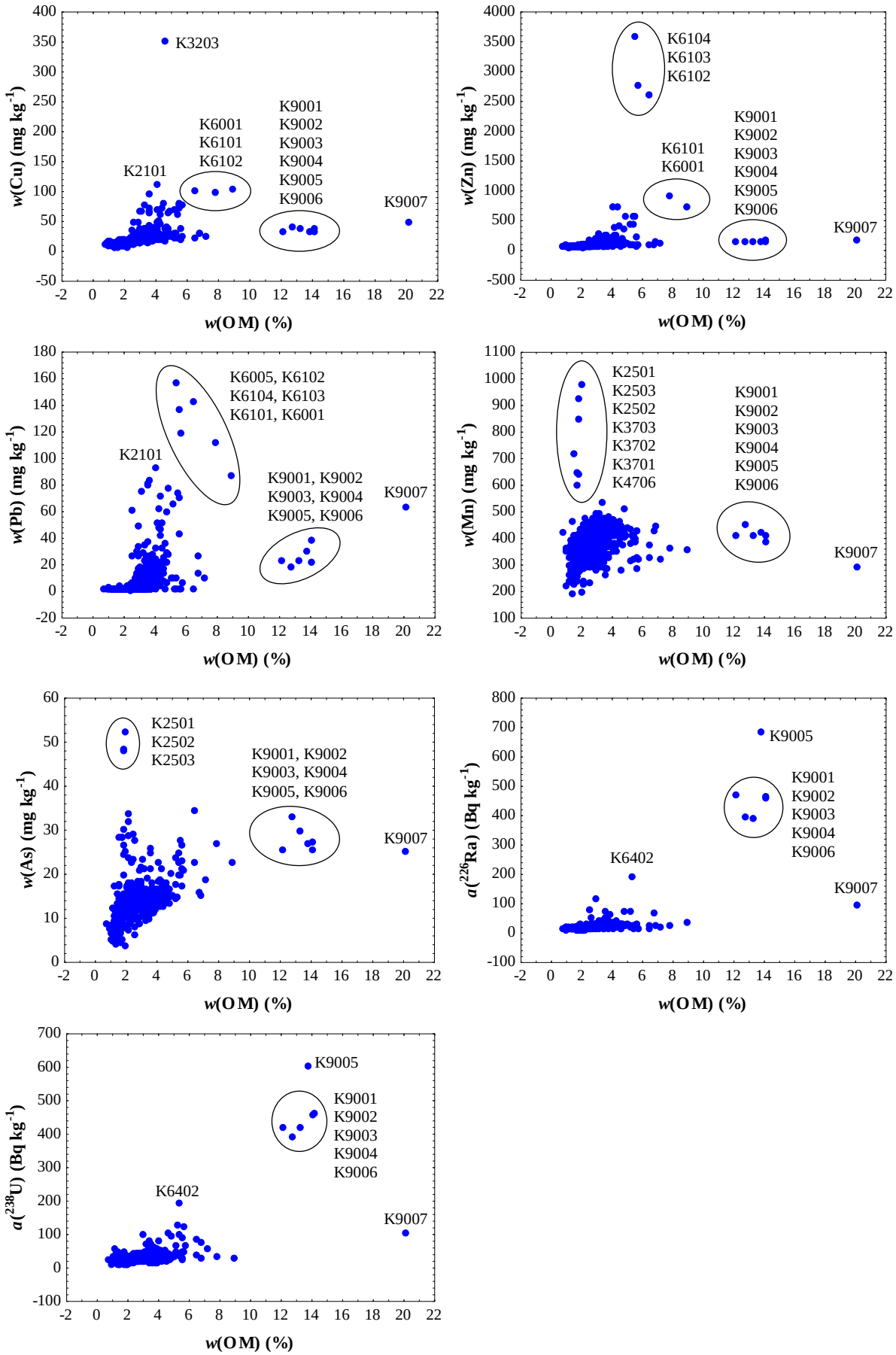
w(Cu) (mg kg-1)
K3203
K6001
K6101
K6102
K2101
K9001
K9002
K9003
K9004
K9005
K9006
K9007
w(OM) (%)
w(Zn) (mg kg-1)
K6104
K6103
K6102
K6101
K6001
K9001
K9002
K9003
K9004
K9005
K9006
K9007
w(OM) (%)
w(Pb) (mg kg-1)
K6005, K6102
K6104, K6103
K6101, K6001
K2101
K9001, K9002
K9003, K9004
K9005, K9006
K9007
w(OM) (%)
w(Mn) (mg kg-1)
K2501
K2503
K2502
K3703
K3702
K3701
K4706
K9001
K9002
K9003
K9004
K9005
K9006
K9007
w(OM) (%)
w(As) (mg kg-1)
K2501
K2502
K2503
K9001, K9002
K9003, K9004
K9005, K9006
K9007
w(OM) (%)
a(226Ra) (Bq kg-1)
K9005
K9001
K9002
K9003
K9004
K9006
K6402
K9007
w(OM) (%)
a(238U) (Bq kg-1)
K9005
K9001
K9002
K9003
K9004
K9006
K6402
K9007
w(OM) (%)

Table 1 Geographical coordinates and sea bottom depths of sampling stations in Kaštela Bay.

Sampling station	Coordinates		Sea bottom depth (m)	Sampling station	Coordinates		Sea bottom depth (m)
	N	E			N	E	
K00	43° 32.495'	16° 19.364'	4,5	K49	43° 30.373'	16° 22.401'	41
K01	43° 32.508'	16° 20.205'	14	K50	43° 30.372'	16° 23.194'	31
K02	43° 32.492'	16° 20.931'	20	K51	43° 30.373'	16° 23.763'	23
K03	43° 32.525'	16° 21.713'	22	K52	43° 29.855'	16° 20.938'	22
K04	43° 32.535'	16° 22.442'	16	K53	43° 29.830'	16° 21.703'	37
K05	43° 32.554'	16° 23.204'	20	K54	43° 29.814'	16° 22.433'	41
K06	43° 32.533'	16° 23.824'	21	K55	43° 29.820'	16° 23.165'	45
K07	43° 32.548'	16° 24.445'	16	K56	43° 29.804'	16° 23.881'	45
K08	43° 32.528'	16° 25.031'	15	K57	43° 29.815'	16° 24.499'	43
K09	43° 32.529'	16° 25.617'	13	K58	43° 29.824'	16° 25.315'	41
K10	43° 31.998'	16° 18.524'	3,5	K59	43° 29.291'	16° 23.884'	50
K11	43° 31.996'	16° 19.349'	15	K60	43° 31.738'	16° 27.988'	12
K12	43° 32.009'	16° 20.177'	22	K61	43° 31.762'	16° 27.556'	14
K13	43° 31.993'	16° 20.917'	30	K62	43° 31.747'	16° 26.633'	15
K14	43° 32.000'	16° 21.707'	32	K63	43° 30.054'	16° 25.344'	14
K15	43° 31.986'	16° 22.431'	33	K64	43° 30.045'	16° 25.040'	32
K16	43° 32.002'	16° 23.203'	32	K65	43° 30.060'	16° 24.748'	34
K17	43° 31.980'	16° 23.868'	33	K66	43° 30.054'	16° 24.516'	35
K18	43° 32.040'	16° 24.431'	30	K67	43° 30.044'	16° 24.200'	40
K19	43° 32.008'	16° 25.160'	14	K68	43° 30.041'	16° 23.877'	41
K20	43° 32.002'	16° 25.892'	28	K69	43° 30.358'	16° 23.344'	33
K21	43° 32.000'	16° 26.655'	17	K70	43° 31.004'	16° 16.703'	8,5
K22	43° 32.006'	16° 27.539'	16	K71	43° 32.940'	16° 21.647'	8,0
K23	43° 31.990'	16° 27.975'	10	K72	43° 32.802'	16° 23.795'	4,0
K24	43° 31.366'	16° 17.676'	8,0	K73	43° 32.526'	16° 24.171'	15
K25	43° 31.445'	16° 18.517'	12	K74	43° 32.529'	16° 24.725'	16
K26	43° 31.452'	16° 19.346'	17	K75	43° 32.523'	16° 25.295'	15
K27	43° 31.484'	16° 20.178'	15	K76	43° 32.287'	16° 24.127'	29
K28	43° 31.466'	16° 20.923'	30	K77	43° 32.260'	16° 24.448'	30
K29	43° 31.476'	16° 21.694'	36	K78	43° 32.287'	16° 24.759'	29
K30	43° 31.463'	16° 22.444'	36	K79	43° 32.259'	16° 24.993'	29
K31	43° 31.439'	16° 23.168'	36	K80	43° 32.270'	16° 25.337'	26
K32	43° 31.444'	16° 23.873'	35	K82	43° 32.661'	16° 25.134'	5,0
K33	43° 31.483'	16° 24.651'	33	K82a	43° 32.616'	16° 25.115'	9,0
K35	43° 30.934'	16° 17.716'	12	K83	43° 32.546'	16° 25.138'	12
K36	43° 30.908'	16° 18.540'	17	K84	43° 32.926'	16° 22.404'	4,0
K37	43° 30.911'	16° 19.361'	14	K85	43° 32.913'	16° 20.889'	7,5
K38	43° 30.868'	16° 20.169'	14	K86	43° 31.460'	16° 16.724'	2,0
K39	43° 30.914'	16° 20.928'	32	K87	43° 31.023'	16° 15.976'	6,0
K40	43° 30.915'	16° 21.704'	38	K88	43° 31.269'	16° 15.954'	1,5
K41	43° 30.902'	16° 22.422'	38	K89	43° 30.394'	16° 19.416'	12
K42	43° 30.900'	16° 23.185'	37	K90	43° 32.699'	16° 25.117'	3,0
K43	43° 30.873'	16° 23.847'	11	K91	43° 32.643'	16° 25.118'	8,0
K44	43° 30.948'	16° 24.685'	3,0	K92	43° 32.590'	16° 25.117'	13
K45	43° 30.966'	16° 25.408'	8,0	KV01	43° 30.703'	16° 19.920'	18
K46	43° 30.386'	16° 20.206'	26	KK	43° 30.588'	16° 22.712'	50
K47	43° 30.392'	16° 20.892'	33	KC	43° 32.236	16° 19.957	12
K48	43° 30.388'	16° 21.668'	34				

Table 2 Basic statistical parameters of radionuclides massic activities (in Bq kg^{-1}) and metals (in mg kg^{-1}) and organic matter (OM, in %) mass fractions in sediments of Kaštela Bay for a depth 0–50 cm; N = 604, N – number of samples, $\bar{x}$ – mean value, SD – standard deviation. Measurement uncertainties are given for mean value, minimum, and maximum; $k = 2$ for $p =$ 95 %. Values are rounded where necessary.

Statistical parameter	**^{40}K**	**^{226}Ra**	**^{232}Th**	**^{238}U**	**^{137}Cs**	**Al**	**K**	**Ca**	**Ti**	**V**	**Cr**	**Mn**
$\bar{x}$	310 ±5	25 ±2	19.2 ±0.3	34 ±2	2.2 ±0.1	30000 ±220	13700 ±130	189000 ±1500	2400 ±11	64.2 ±0.6	69.7 ±0.4	390 ±3
SD	140	48	6.5	46	2.3	5500	3200	36100	280	13	9.9	73
Minimum	15 ±8	5.4 ±1.0	5.1 ±0.7	6.7 ±7.7	0.1 ±0.2	19000 ±5500	4000 ±480	91000 ±22000	1500 ±20	36 ±2	38 ±3	190 ±3
Maximum	540 ±28	690 ±14	43 ±3	600 ±36	12 ±1	45000 ±13000	18700 ±2200	315000 ±77000	3400 ±50	180 ±11	190 ±14	970 ±18
Median	320	20	19	28	1.0	29000	14000	185000	2500	66	71	400
Statistical parameter	**Fe**	**Co**	**Ni**	**Cu**	**Zn**	**Ga**	**Rb**	**Sr**	**Y**	**Pb**	**As**	**OM**
$\bar{x}$	21300 ±160	8.57 ±0.03	43.9 ±0.4	21.7 ±0.8	110 ±9	7.7 ±0.1	64 ±1	370 ±6	10.8 ±0.3	8.7 ±0.7	14.4 ±0.2	3.1 ±0.1
SD	3800	0.80	11	19	220	2.5	24	150	8.2	18	4.8	1.6
Minimum	10600 ±140	6.6 ±0.1	19 ±2	5.2 ±0.5	43 ±2	2.3 ±0.2	11.8 ±0.4	200 ±4	< 1.0	< 1.6	3.7 ±0.2	0.77 ±0.03
Maximum	35600 ±480	12.1 ±0.3	88 ±10	350 ±36	3600 ±180	14 ±1	100 ±4	890 ±17	46 ±10	160 ±18	52 ±3	20.2 ±0.03
Median	21700	8.6	44	19	83	7.8	67	320	10	2.0	14	3.0

Table 3 Mineral composition of sediment at KK (0–50 cm) and KC (0–30 cm) sampling stations and in K9005 sample (20–25 cm); +++ significantly abundant (approx. 25–40 %), ++ considerably abundant (approx. 10–25 %), + subordinate to accessory (< 10 %), - not present.

Mineral/Chemical formula	**Sampling station/Sample**		
	KK	**KC**	**K9005**
Calcite, $CaCO_3$	+++	+++	+++
Quartz, SiO_2	++	++	++
Aragonite, $CaCO_3$	-	+	-
Halite, NaCl	+	+	+
Muscovite, $(K,Na)(Al,Mg,Fe)_2(Si_3Al)O_{10}(OH)_2$	+	+	-
Chlorite, $(Mg,Fe,Al)_6(Si,Al)_4O_{10}(OH)_8$	+	+	-
Hematite, Fe_2O_3	-	-	+
Magnesium calcite, $(Mg_{0,129}Ca_{0,871})CO_3$	-	-	++
Illite/muscovite, $(Na_{0,07}K_{0,90}Ba_{0,01})(Al_{1,84}Ti_{0,04}Fe_{0,07}Mg_{0,04})(Si_{3,02}Al_{0,98})O_{10}(OH)_2$	-	-	++
Pyrite, FeS_2	-	-	+

Table 4 Correlation matrix for radionculides massic activities, metals mass fractions and organic matter (OM) mass fractions in sediment of Kaštela Bay for a depth 0–50 cm; N = 587, N – number of samples, marked correlations are significant at $p < 0.05$, 0.00 to ±0.20: no or slightly correlated (in blue), ±0.20 to ±0.40: weak correlation (in yellow), ±0.40 to ±0.70: real significant correlation (in green), ±0.70 to ±1.00: high or very high correlation (in red).

	^{40}K	^{137}Cs	^{226}Ra	^{232}Th	^{238}U	Al	K	Ca	Ti	V	Cr	Mn	Fe	Co	Ni	Cu	Zn	Ga	Rb	Sr	Y	Pb	As	OM
^{40}K	1.00																							
^{137}Cs	0.37	1.00																						
^{226}Ra	0.28	0.28	1.00																					
^{232}Th	0.95	0.21	0.25	1.00																				
^{238}U	0.27	0.12	0.57	0.25	1.00																			
Al	0.78	0.31	0.15	0.70	0.02	1.00																		
K	0.94	0.32	0.24	0.88	0.22	0.83	1.00																	
Ca	-0.93	-0.39	-0.28	-0.86	-0.23	-0.77	-0.92	1.00																
Ti	0.95	0.40	0.30	0.89	0.23	0.80	0.96	-0.95	1.00															
V	0.88	0.45	0.36	0.81	0.36	0.74	0.89	-0.90	0.92	1.00														
Cr	0.72	0.41	0.33	0.65	0.24	0.58	0.71	-0.75	0.77	0.71	1.00													
Mn	0.72	0.25	0.26	0.68	0.13	0.60	0.71	-0.70	0.73	0.67	0.67	1.00												
Fe	0.94	0.42	0.30	0.86	0.24	0.81	0.97	-0.95	0.97	0.94	0.76	0.75	1.00											
Co	0.93	0.41	0.29	0.86	0.22	0.82	0.95	-0.93	0.95	0.92	0.74	0.75	0.98	1.00										
Ni	0.73	0.29	0.30	0.66	0.30	0.64	0.72	-0.68	0.72	0.71	0.63	0.61	0.73	0.73	1.00									
Cu	0.34	0.48	0.26	0.26	0.19	0.12	0.30	-0.34	0.35	0.42	0.36	0.26	0.40	0.39	0.30	1.00								
Zn	0.25	0.46	0.15	0.19	0.10	0.06	0.22	-0.25	0.26	0.34	0.30	0.16	0.30	0.30	0.21	0.78	1.00							
Ga	0.94	0.35	0.26	0.87	0.24	0.81	0.93	-0.91	0.93	0.88	0.70	0.70	0.94	0.93	0.73	0.29	0.21	1.00						
Rb	0.97	0.38	0.25	0.90	0.27	0.80	0.96	-0.94	0.96	0.91	0.72	0.69	0.96	0.95	0.74	0.35	0.26	0.95	1.00					
Sr	-0.82	-0.35	-0.33	-0.77	-0.20	-0.57	-0.74	0.72	-0.78	-0.66	-0.67	-0.61	-0.73	-0.73	-0.58	-0.37	-0.28	-0.74	-0.77	1.00				
Y	0.42	0.13	0.22	0.46	0.18	0.22	0.36	-0.36	0.44	0.36	0.44	0.41	0.38	0.37	0.51	0.17	0.07	0.40	0.42	-0.45	1.00			
Pb	0.19	0.51	0.18	0.11	0.09	-0.00	0.15	-0.19	0.20	0.29	0.24	0.14	0.25	0.26	0.17	0.83	0.83	0.14	0.20	-0.25	0.06	1.00		
As	0.16	0.13	0.08	0.17	0.18	0.10	0.21	-0.28	0.23	0.39	0.20	0.26	0.33	0.30	0.15	0.33	0.32	0.19	0.21	0.06	0.04	0.34	1.00	
OM	0.64	0.57	0.40	0.52	0.48	0.42	0.58	-0.66	0.64	0.73	0.55	0.40	0.67	0.66	0.56	0.59	0.54	0.60	0.67	-0.51	0.24	0.49	0.37	1.00

Table 5 Correlations of radionuclides massic activities, metals mass fractions, and organic matter (OM) mass fractions with grain size in sediment at KK and KC sampling stations of Kaštela Bay for a depth 0–50 cm; N = 14, N – number of samples, GR – gravel, SA – sand, SL – silt, CL – clay, marked correlations are significant at $p < 0.05$, 0.00 to ±0.20: no or slightly correlated (in blue), ±0.20 to ±0.40: weak correlation (in yellow), ±0.40 to ±0.70: real significant correlation (in green), ±0.70 to ±1.00: high or very high correlation (in red).

	^{40}K	^{137}Cs	^{226}Ra	^{232}Th	^{238}U	Al	K	Ca	Ti	V	Cr	Mn	Fe	Co
GR	**-0.94**	-0.50	**-0.83**	**-0.92**	**-0.88**	0.43	**-0.93**	**0.91**	**-0.90**	**-0.90**	**-0.81**	**-0.93**	**-0.93**	**-0.94**
SA	**-0.99**	-0.49	**-0.85**	**-0.98**	**-0.90**	0.47	**-0.99**	**0.99**	**-0.98**	**-0.96**	**-0.90**	**-0.99**	**-0.99**	**-0.97**
SL	**0.99**	0.53	**0.87**	**0.97**	**0.91**	-0.45	**0.99**	**-0.98**	**0.98**	**0.96**	**0.91**	**0.99**	**0.99**	**0.98**
CL	**0.99**	0.45	**0.84**	**0.98**	**0.89**	-0.47	**0.98**	**-0.98**	**0.97**	**0.95**	**0.86**	**0.99**	**0.98**	**0.96**
	Ni	**Cu**	**Zn**	**Ga**	**Rb**	**Sr**	**Y**	**Pb**	**As**	**OM**	**GR**	**SA**	**SL**	**CL**
GR	**-0.86**	**-0.79**	**-0.73**	**-0.86**	**-0.93**	**0.88**	**-0.86**	**-0.68**	-0.52	**-0.81**	1.00	**0.93**	**-0.94**	**-0.96**
SA	**-0.95**	**-0.88**	**-0.80**	**-0.94**	**-1.00**	**0.98**	**-0.90**	**-0.71**	**-0.56**	**-0.84**	**0.93**	1.00	**-1.00**	**-0.99**
SL	**0.94**	**0.89**	**0.82**	**0.94**	**0.99**	**-0.98**	**0.90**	**0.75**	**0.56**	**0.86**	**-0.94**	**-1.00**	1.00	**0.99**
CL	**0.95**	**0.85**	**0.77**	**0.92**	**0.99**	**-0.97**	**0.90**	**0.68**	**0.55**	**0.82**	**-0.96**	**-0.99**	**0.99**	1.00